Task 9. Cobalt Catalyst Life Testing

The objective of this task is to obtain life data on baseline cobalt Fischer-Tropsch catalysts.

A. Deactivation Study of Co-Re-Al_2O_3 Catalysts

It becomes more likely that, for the short term, the feed gas for a commercial Fischer-Tropsch synthesis operation will be based on natural gas instead of coal; therefore, cobalt catalysts may be preferred. Due to the high cost of cobalt catalysts, a stable catalyst is required to ensure extended runs. Thus, the cobalt catalyst must either be amenable to frequent regenerations over a long catalyst life or it must have a stable catalytic activity over a long (year or longer) period of time. A fundamental understanding of the deactivation mechanisms of cobalt catalysts is thus required to develop understanding that leads to the preparation of more stable catalysts and also to select the operating conditions to extend catalyst lifetime.

Supported cobalt catalysts deactivate during extended periods of time and commonly accepted reasons include: oxidation, carbon deposition, sintering, and sulfur poisoning. Sulfur poisoning can be avoided by deep desulfurization of the feed gas (at the expense of increases in the cost of synthesis gas). Carbon deposition may be minimized by careful control of the temperature protocol. The deactivation caused by sintering and oxidation will therefore be the major concerns. Investigations of the mechanism become very important.

Thermodynamically, bulk oxidation of cobalt to cobalt oxide by water is not favored under the reaction conditions (220°C, 275 psig, H_2:CO=2:1, 50-70% CO conversion). However, there are numerous literature citations to support the view that oxidation of supported catalysts occurs under the reaction conditions. A common belief is that the smaller the cobalt crystal size, the easier the oxidation. Thus, there may be a "magic" dispersion limit where, if the cobalt

dispersion is higher than the "magic" number, oxidation takes place very rapidly, resulting in rapid catalyst deactivation. Another hypothesis is that although bulk oxidation is unlikely, surface oxidation of the cobalt could occur during Fischer-Tropsch synthesis and this would also cause rapid catalytic activity decline.

The objective of the current study is to define the deactivation rate of the Co-Re-Al_2O_3 catalysts at different space velocities, to study the deactivation mechanism, to learn whether the deactivation is caused by sintering of the cobalt crystals, the oxidation of cobalt to cobalt oxide or the formation of cobalt aluminate.

Experimental

Catalysts. Three catalysts with a cobalt loading of 15 wt.% and rhenium loading of 0.2, 0.5 and 1.0 wt.%, respectively, were utilized.

Activation. The catalysts were reduced using 30 % H_2/70% He (V/V) in a fixed bed reactor at a space velocity of 10,000 GHSV at 350°C. The temperature was ramped to 350°C at 1°C per minute and held at 350°C for 4 hours. This was accomplished by overpressuring the reduction tube that contains the reduced catalyst and then opening the appropriate valves to force the entire catalyst volume into the autoclave containing the startup solvent. The reduction reactor was weighed prior to and after catalyst transfer to ensure that a quantitative transfer of the catalyst had been accomplished. The catalyst was then treated in hydrogen flow in the slurry phase reactor at 280°C for 4 hours.

Reaction Conditions. About 20 grams (actual catalyst weight for each run was accurately known) of catalyst was transferred into a 1L stirred autoclave which had been charged with 300g of C_{30} oil (decene trimer obtained from Ethyl Corp.). Following catalyst reduction at 280°C in situ, the temperature was lowered to 150°C and synthesis gas was fed into the reactor. After the

pressure reached 275 psig, the temperature was slowly increased to 220°C during 4 hours. A feed gas with H_2:CO ratio of 2:1 was used.

Results and Discussion

The activity and rate of loss of activity data are shown in figures 1 through 3. The activity measurements for the first two runs (using the two lower Re loaded catalysts) were started at 2.0 SL/g. cat./hr. Considering the scatter of the initial data for the run with the catalyst containing 0.5 wt.% Re (figure 2), the initial conversions for the 0.2 and 0.5 wt.% Re catalysts were essentially the same (70-75% CO conversion). These two catalysts exhibited a rapid and similar deactivation rate of the range 12-14% CO conversion/week. The catalyst containing 1.0 wt.% Re was started up at a higher flow rate so that the initial CO conversion was lower (37% compared to 70-75%) and the activity decline rate was lower (4.35 %CO conversion/week). Extrapolating the linear relation of the space velocity versus conversion data, described later, for these three catalysts, the initial conversion of CO with the 1% Re catalyst at a GHSV of 2.0 SL/g. cat/hr, as was used with the 0.2 and 0.5 wt.% Re catalysts, indicate an initial conversion of 95%. Considering the uncertainty associated with this extrapolation, a tentative conclusion is that the three catalysts with different Re content would have had a similar initial conversion for identical reaction conditions.. However, additional runs are required to better define this, and these will be done during the next quarter.

To establish a deactivation rate to cover a wide range of conversion levels will be a challenge. First, consider the data for the 0.2% Re catalyst. During the initial portion of the run at a space velocity of 2.0 SL/g. cat./hr, the rate of decline is high at 14.1% CO/week during about the first 200 hours of synthesis time. Returning to the same space velocity at about 700 hours of operation yielded a rate of decline that was much lower (figure 1); the rate of decline after

returning to this same space velocity at about 1700 hours of synthesis is only 1.64% CO conversion/week. Compare the rate of decline of 4.61 %CO conversion/week when operating at 5 SL/g. cat./hr (during about 200-700 hours) with a conversion range of about 12-25% CO to the rate at 2.0 SL/g. cat./hr of 1.64 %CO conversion/week at about 1700 to 2300 hours with a range of about 27-33% CO conversion. If the rate of decline was determined only by the conversion level, the rate at 2.0 L/g. cat./hr (1.64) should have been greater than the one at 5.0 L/g. cat./hr (4.61), and this was not the case. It therefore appears that time on stream may be as important, or even more important, than the conversion level. This has been observed with our Co-SiO_2 catalyst and has been reported by Sasol workers [1]. The Sasol workers, operating for a long period of time at the same operating conditions, have shown a rapid rate of decline in conversion during the initial synthesis period that is followed by a much longer period with a much smaller rate of decline (figure 4). The data for the 1% Re catalyst also appear to be consistent with this concept. These data are summarized in Table 1.

After more than 1800 hours of synthesis, regeneration (rejuvenation) was attempted with the catalyst containing 1% Re. The first rejuvenation was at reaction temperature with a H_2 flow rate of 7.5 SL/g. cat./hr and resulted in regaining 49% of the initial activity (figure 5) but this was followed by a rapid decline in CO conversion. The second rejuvenation was conducted at reaction temperature and pressure but at double the total flow (15 SL/g. cat./hr; H_2:Ar = 1:1) and for 4 hours. The second rejuvenation returned the CO conversion to 66% of the initial activity. However, during less than two days of operation, the CO conversion declined to about 40% of the initial activity. Following this rapid decline, there was a slower, but still high, rate of decline of about 17 %CO conversion/week.

Similar studies are continuing.

References

1. P. J. van Berge and R. C. Everson, Natural Gas Conversion. IV, (M. dePontes, et al., eds) Studies in Surface Science and Catalysis, **107**, 207 (1997).

Table 1 Deactivation Rate, % CO conversion/week				
Promoter Level, wt.%	Rate	%CO conversion range	Rate	%CO conversion range
0.2	4.61	12-25	14.1	55-75
0.5	---	---	12.3	18-70
4.35	4.35	11-38	---	---

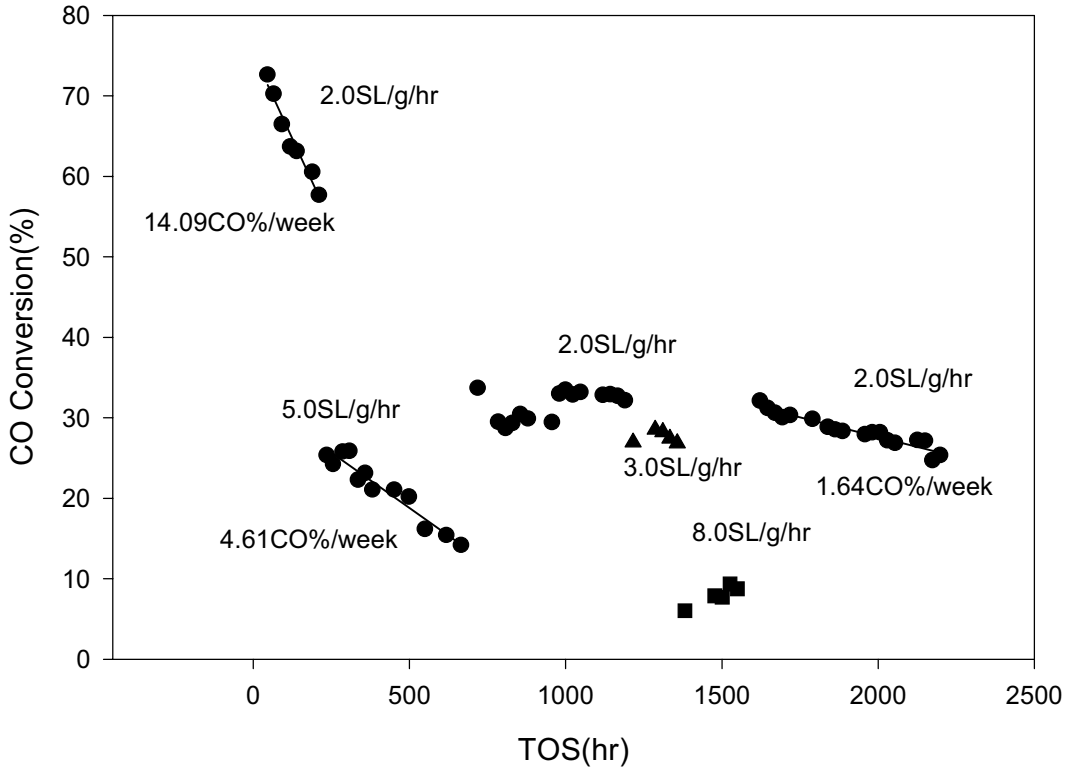

Fig 1 CO Conversion as a function of time on stream on 15%Co-0.2%Re/Al_2O_3

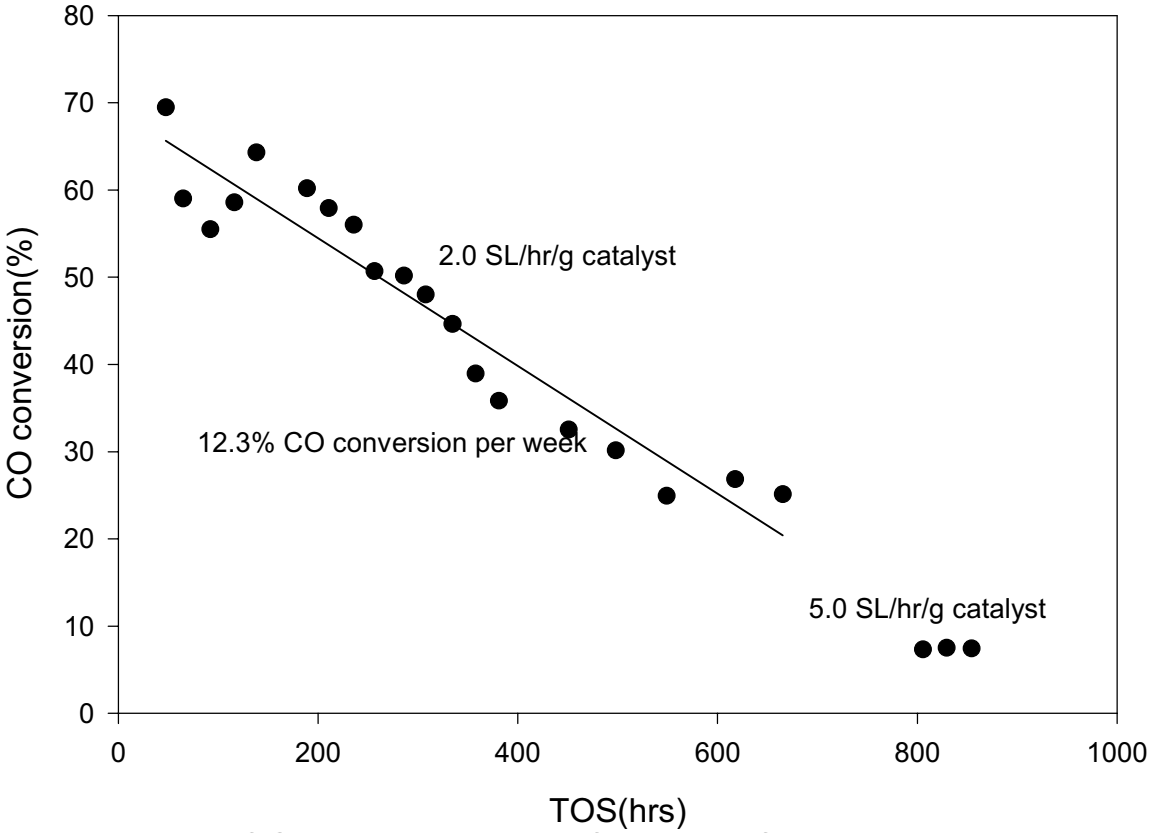

Fig 2 CO conversion as a function of time on stream for 15%Co-0.5%Re/Al_2O_3 catalyst, regenerate at 220^0C, just stop the CO flow for 24hrs(too long) has no recovery, regenerate at 280^0C, activity goes up close to the initial activity, but the product was mainly methane

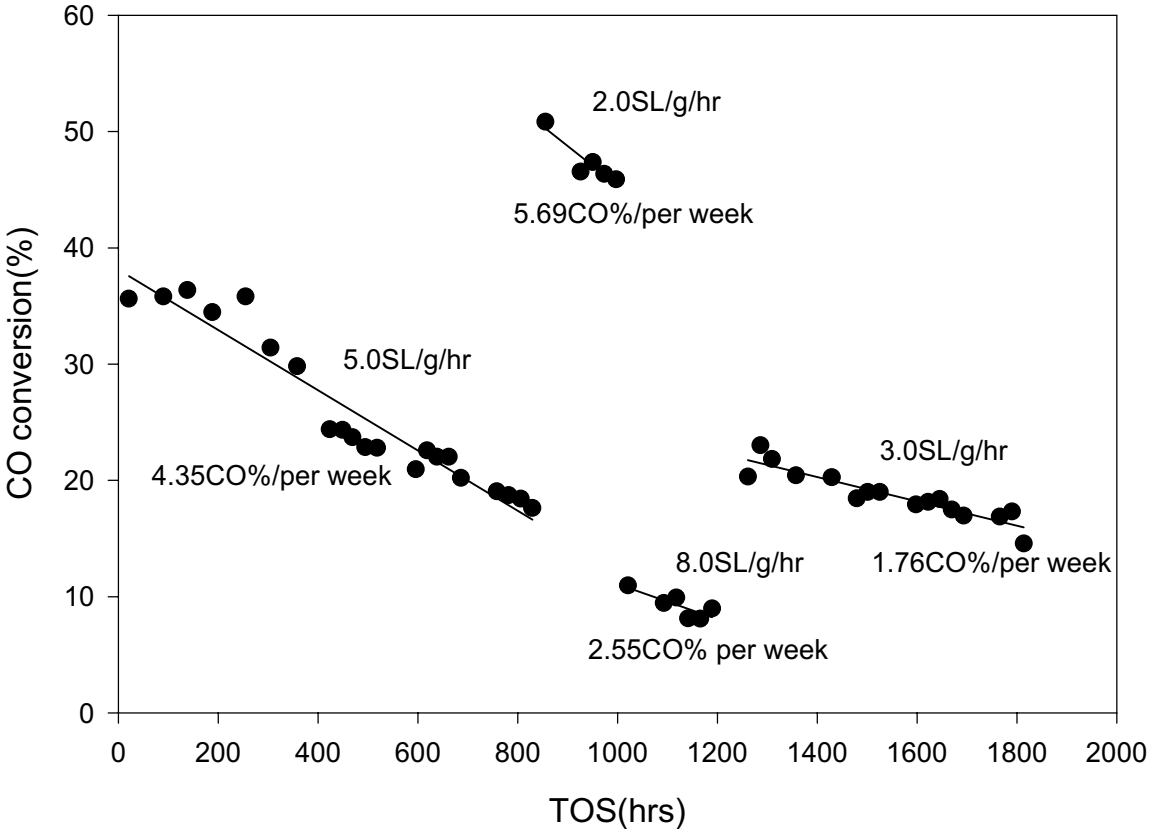

Fig 3 CO conversion as a function of time on stream for 15%Co-1%Re/Al_2O_3 catalyst

FIGURE 4. STABILITY RUN ON THE COBALT CATALYST

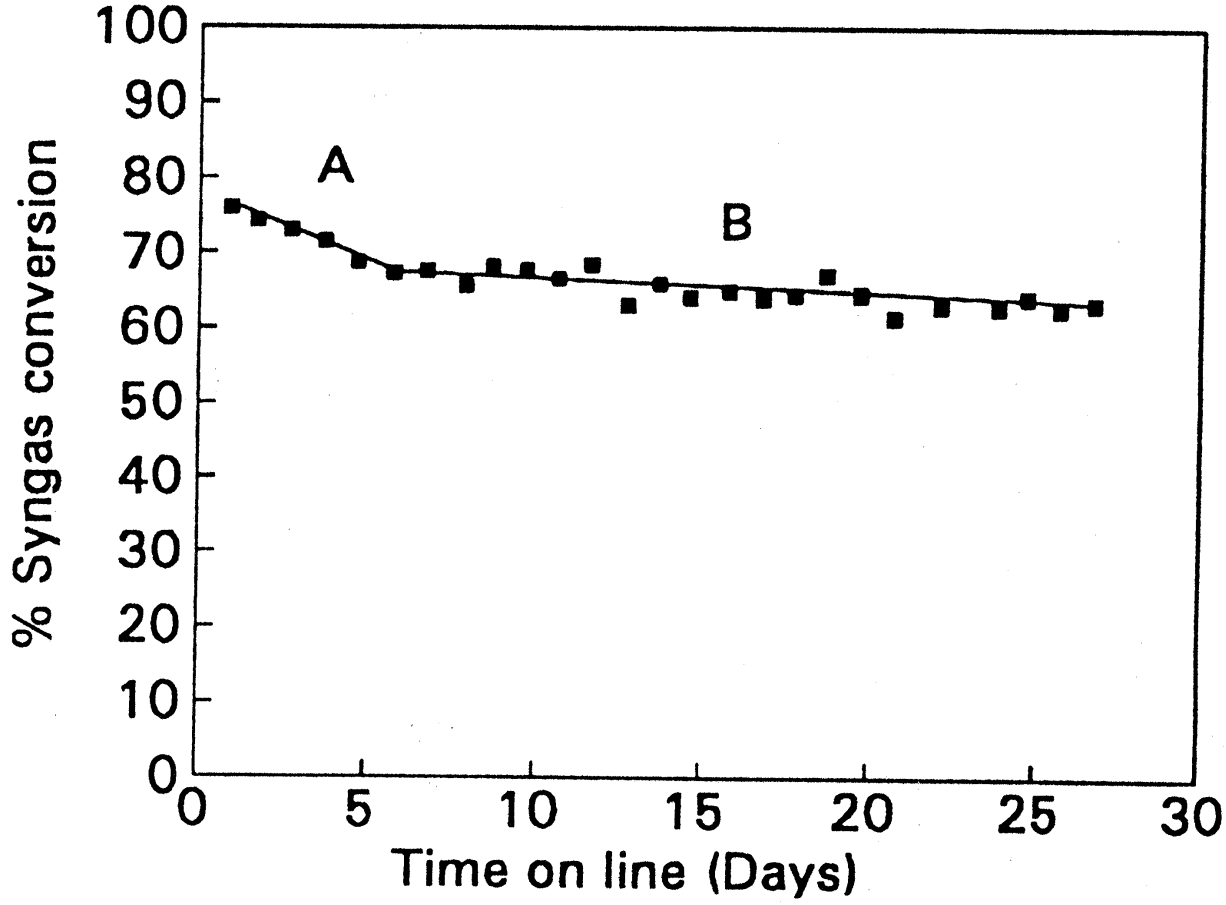

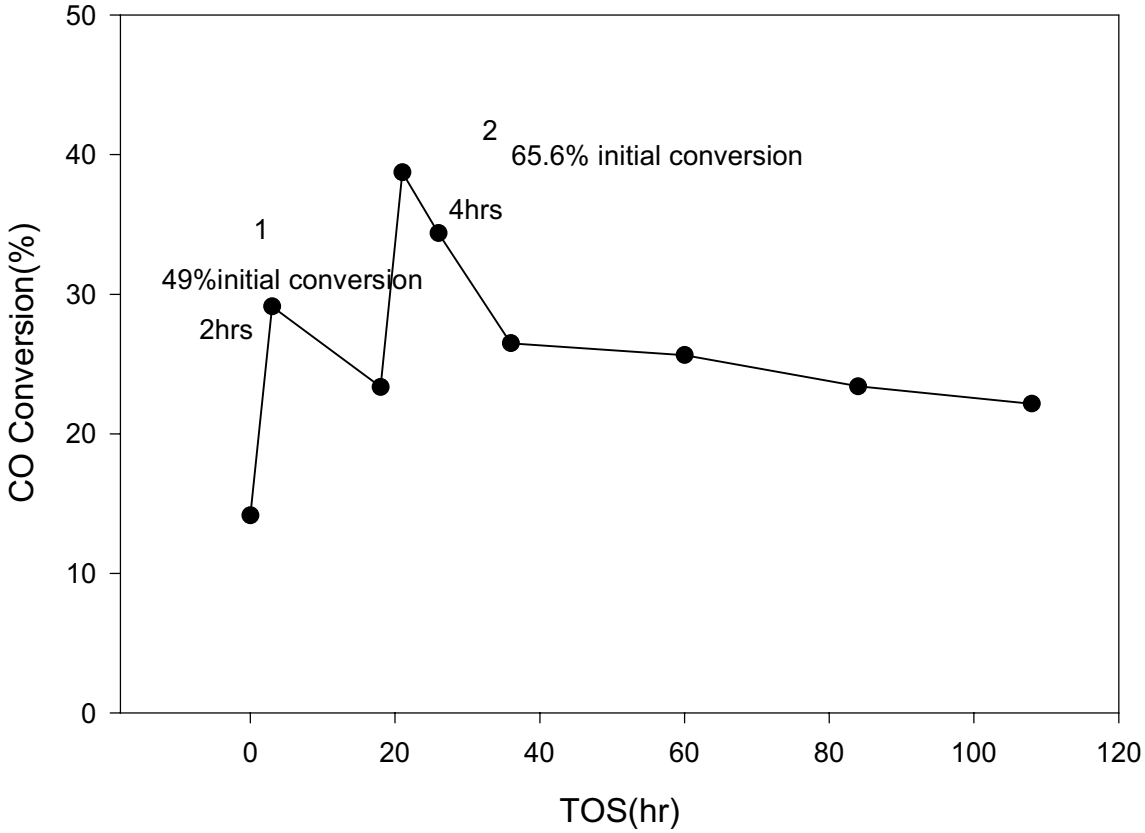

Fig 5 Rejuvenation of catalyst 15%Co-1%Re/Al_2O
1: rejuvanate by H2(7.5SL/hr/g), 2: rejuvenate
by H2 and Ar mixture(H2:Ar)=1:1, 15SL/g/hr)

Task 10. Cobalt Catalyst Mechanism Study

The objective of this task is to determine the impact of secondary reactions on the relationship of cobalt Fischer-Tropsch catalysts under conditions appropriate to slurry bubble column reactors.

A. Product Distribution of Fischer-Tropsch Synthesis

Fischer-Tropsch (FT) synthesis can be conducted in either vapor phase or vapor-liquid reactors depending on the product demand and the catalyst performance. Vapor phase reactors feature high temperature operation (>300^{o}C) and low alpha products (e.g., gasoline). Single alpha is a common observation with this type of operation. When high alpha products are the goal (e.g., diesel, wax), the synthesis is typically carried out in fixed-bed or slurry bubble column reactors at low temperature (<250 ^{o}C). In these reactors, products are separated into vapor and liquid two phases, and a two alpha product distribution has been observed in both laboratory and pilot scale tests. With the assumption that chain growth follows the so-called ASF single alpha chemistry on the surface, several models have been proposed to explain the two alpha observation, including: two active sites that are responsible for different chain growths, diffusion enhanced olefin readsorption in catalyst pores, and the effect of vapor-liquid-equilibrium (VLE) which causes accumulation of heavier products in the reactor and thus enhances olefin reactivity.

In most FT reactors, when vapor liquid separation is involved, the sample taken is actually not representative of what is produced during the sampling period, unless an impractically long time is taken for the reactor to reach “steady state”. This sampling behavior has been suspected to be responsible for the two alpha product distribution due to VLE of products in the reactor. Recently, we have proved that, without considering the reactivity of

olefin products, simple accumulation effect of heavier products by VLE cannot be responsible for the two alpha observation in a slurry reactor under normal operating conditions (1).

It is generally agreed that the reversible olefin termination path is responsible for the two alpha product distribution. Yet, there is still significant dispute in how this reversible reaction works. The diffusion enhanced olefin readsorption model attributes the two alpha observation to increasing internal diffusion limitations of the olefin products due to reduced diffusivity with increasing carbon number. However, this model ignores the presence of a liquid phase in which the catalyst resides. Our recent work indicated that the internal diffusion limitation of hydrocarbon products does not necessarily exist in catalyst pores unless there is also an internal diffusion limitation of reactants (2). Also, due to the effect of vapor-liquid separation of hydrocarbon products in the reactor, the severity of diffusion limitation of light hydrocarbons (C_{20-}) actually decreases with increasing carbon number, just opposite to the cornerstone assumption of the diffusion model. Consequently, it was concluded that internal diffusion of products could not be responsible for the two alpha distribution, even though it might alter the alpha value.

The effect of VLE on the two alpha product distribution has been proposed by a few researchers, although it was also rejected by other researchers (3). The basic idea of this model is that the higher olefin carbon number, the longer the residence time in the reactor and therefore the greater the contribution of the reversible olefin reaction. As a result, product distribution appears as a function of carbon number. In this work, we demonstrate conceptually that the two alpha observation could be due to the effect of VLE when considering olefin reactivity. For simplicity of discussion, a continuously stirred tank reactor (CSTR) is used for this modeling

study. Nonetheless, the same method can be applied to any type of reactor, as long as there is vapor-liquid separation of products.

Reaction Pathway and Model Development

The Fischer-Tropsch synthesis is a very complicated reaction and the reaction mechanism is virtually unknown. Over the years it has been recognized that a simple polymerization mechanism should describe the product distribution, with surface chain growth intermediate being paraffinic or olefinic species. For the purpose of qualitatively understanding the product distribution, it is unimportant to distinguish the type of surface intermediate because both of them lead to the same dependency on carbon number. In this work, it is assumed that the chain growth follows the pathways shown in Figure 1, ignoring minor side reactions such as alcohol production. It is also assumed that there is only one type of active site on catalyst surface on which any surface process takes place. According to this scheme, the chain growth intermediate grows by addition of surface methylene species, terminates to paraffin by hydrogenation or to olefin by β- abstraction of hydrogen. The termination path to paraffin is irreversible since paraffins are non-reactive under typical FT conditions, while the pathway to olefin is reversible. Surface olefin species can undergo half hydrogenation reversibly to form a surface chain growth intermediate or desorption as a free olefin molecule in the catalyst pores. The latter can adsorb reversibly on the catalyst surface or diffuse out of catalyst pores and be removed as reaction product.

The physical adsorption of olefins on the catalyst surface was taken into account by some researchers when modeling FT product distribution (4,5). This factor is not considered in this work since the effect of physical adsorption is virtually the same as that of liquid condensation and wetting. In the presence of vapor-liquid separation, the catalyst pores are filled with liquid

which causes the physical adsorption layer in the vicinity of catalyst surface to vanish. Nevertheless, chemisorption of olefin may have a significant effect on product distribution. As a rule of thumb, other factors being equal, one may expect that the degree of chemical adsorptivity will increase with increasing molecular weight. However, since very little quantitative data are available for olefin chemisorption and the objective of this work is solely aimed at the effect of VLE, the olefin adsorption and desorption rate constants are assumed to be independent of carbon number.

Figure 2 shows schematically a typical CSTR slurry reactor, in which unconverted reactants and hydrocarbon products are separated into two phases, liquid and vapor. Both liquid and vapor products are removed continuously to maintain constant liquid level in the reactor. With the assumption that there is no internal diffusion limitation of reactants, the diffusion of hydrocarbon products in the catalyst pores is not considered, as has been proved to be absent (2). Based on the reaction mechanism of Figure 1, the steady state material balance of each surface species of carbon number n is as follows, assuming that the reaction rate constants are independent of carbon number.

Chain growth intermediate C_n^* : $$k_p S_1 S_{n\text{-}1} + k_o' S_H S_{n=} = (k_p S_1 + k_H S_H + k_o) S_n \quad (1)$$

Surface olefin $C_{n=}^*$: $$k_o S_n + k_a x_{n,o} = (k_o' S_H + k_d) S_{n=} \quad (2)$$

Olefin O_n : $$V_R k_d S_{n=} = V_R k_a x_{n,o} + V y_{n,o} + L x_{n,o} \quad (3)$$

Paraffin P_n : $$V_R k_H S_H S_n = V y_{n,p} + L x_{n,p} \quad (4)$$

From the above material balance equations, the concentration ratios of olefin to paraffin in the liquid phase (f_n) and the chain propagation probability on surface (α_n) can be derived as Equations (5) and (6), respectively.

$$f_n = \frac{x_{n,o}}{x_{n,p}} = \frac{k_o k_d}{k_H S_H \left(k_d + k_o' S_H (1+\tau_n k_a)\right)} \tag{5}$$

$$\alpha_n = \frac{S_n}{S_{n-1}} = \frac{1}{1+\beta(1+f_n)} \tag{6}$$

where

$$\beta = \frac{k_H S_H}{k_p S_1}; \quad \tau_n = \frac{V_R}{VH_n + L}; \quad H_n = \frac{y_{n,o}}{x_{n,o}} = \frac{y_{n,p}}{x_{n,p}} = \frac{P_n^s}{P} \tag{7}$$

In Equation (7), τ_n is the average residence time of hydrocarbon product species n, H_n is the ideal vapor-liquid equilibrium constant of hydrocarbon product species n, and β is characteristic of surface propagation probability at high carbon numbers when olefin production rates approach zero. Under the latter situation, the product propagation probability (α_∞) appears to be independent of carbon number, as shown in Equation (8).

$$\alpha_\infty = \frac{k_p S_1}{k_p S_1 + k_H S_H} = \frac{1}{1+\beta} \tag{8}$$

It is clear from Equation (6) that, due to the effect of vapor liquid separation and olefin reactivity, the surface chain propagation probability does not remain constant as proposed by Anderson (6). Instead, it is a decreasing function of olefin to paraffin ratio or an increasing function of carbon

number. Generally, the higher the carbon number, the lower the vapor liquid equilibrium constant (H_n), the higher the average residence time (τ_n), the lower the olefin to paraffin ratio (f_n), and thus the higher the surface propagation probability (α_n).

In practice, it is impossible to collect hydrocarbon products directly from the catalyst surface. The product distribution is obtained by measuring vapor and liquid products collected at the reactor outlet. The production rate of a hydrocarbon species, n, including olefin and paraffin, is:

$$r_n = V(y_{n,p} + y_{n,o}) + L(x_{n,p} + x_{n,o}) = V_R k_H S_H (1 + f_n) S_n \tag{9}$$

and the observed product distribution is

$$\alpha_n' = \frac{r_n}{r_{n-1}} = \frac{1 + f_n}{1 + f_{n-1}} \frac{S_n}{S_{n-1}} = \frac{1 + f_n}{1 + f_{n-1}} \frac{1}{1 + \beta(1 + f_n)} = \lambda_n \alpha_n \tag{10}$$

Equations (5), (6), and (10) completely describe the observed product distribution of Fischer-Tropsch synthesis in a CSTR reactor. In integral reactors, such as a fixed-bed reactor, the molar flowrates of liquid and gas are local values and integration along the reactor bed is necessary before the hydrocarbon production rate at the reactor outlet can be obtained.

Model Simulation and Discussion

The observed alpha value defined in Equation (10) is the one people use to measure FT product distribution. It consists of two parts: the surface chain propagation probability (α_n) and the effect of olefin reincorporation (λ_n). Both of these two factors increase with increasing carbon number, leading to the observed two alpha distribution. In the high carbon number range, f_n approaches zero and λ_n approaches unity. Thus, α_n' appears as a constant, α_∞. This is the so-called second alpha, as it has been named by many researchers. It should be noted that olefin

reincorporation affects the product distribution in the low carbon number range rather than that in the high carbon number range. The so-called "second alpha", α_∞ in this work, reflects the "should be" product distribution rather than the result of olefin reincorporation. For instance, for those catalysts having strong hydrogenation ability, f_n could be very small even for low carbon number species. The effect of olefin reincorporation is insignificant under this situation since f_n is essentially much smaller than unity. As a result, the product distribution, α_n', appears to follow single alpha which is α_∞.

Equation (10) indicates that the observed FT product distribution can be quantified simply using two parameters: olefin to paraffin ratio (f_n) at each carbon number and the β value which can be determined with high carbon number data. In most cases, even at high conversions, the molar flowrate of liquid product at the reactor outlet is significantly lower than that of gas (hydrocarbon products, water, unconverted reactants). Simple flash calculation indicates that this ratio (L/V) is generally less than 0.03 even when CO conversion is 100%. Therefore, the residence time, τ_n, can be approximated with Equation (11) by ignoring the liquid flow rate.

$$\tau_n = \frac{V_R}{VH_n} = \frac{V_R P}{VP_n^s} \tag{11}$$

At high carbon numbers, H_n becomes so small that the magnitude of VH_n could be comparable with that of L. However, ignoring L has negligible effect on α_n' since the magnitude of VH_n is very small and f_n is also very small (close to zero).

For simplicity of simulation, it is further assumed that olefin adsorption/desorption ($C_{n=}$/ $C_{n=}^*$) and hydrogen abstraction of chain growth intermediate/ half hydrogenation of surface olefin($C_n^*/C_{n=}^*$) steps are in equilibrium (Figure 1). This is particularly true at high conversions when the total flow rate at the reactor outlet is lower. With these assumptions, the product

removal is slow ($1/\tau_n << k_o, k_o', k_a, k_d$). Equation (5) reduces to Equation (12), suggesting that the olefin to paraffin ratio is simply proportional to the reciprocal of the average residence time τ_n. In other words, f_n decreases exponentially with carbon number as it is related to the saturated vapor pressure.

$$f_n = \frac{x_{n,o}}{x_{n,p}} = \frac{K_E}{k_H S_H^2 K_{ad} \tau_n} \tag{12}$$

If the above mentioned equilibria are not valid, as can be seen from Equation (5), the dependency of f_n on carbon number is weaker than exponentially for low carbon numbers. The higher the carbon number, the more τ_n dominates the denominator of Equation (5), and therefore the closer the dependency of f_n on carbon number and to the exponential rule.

The model described with Equations (10)-(12) were tested using data obtained from the literature (7). The reaction conditions and major results are summarized in Table 1. The model simulation was performed with experimental data of temperature, α_∞,, and f_3. As shown in Figures 3 and 4, there is a tight fit between model prediction and experimental data for both olefin to paraffin ratio (Figure 3) and product distribution (Figure 4).

In addition to being able to predict the product distribution, a good model should also be capable of explaining some common experimental observation. According to the model developed in this work, the product distribution deviates from single alpha rule for light hydrocarbon products due to the effect of olefin reincorporation. The deviation becomes weaker and weaker with increasing carbon number. Starting at some carbon number and thereafter, the alpha value appears to be constant (α_∞)when the olefin to paraffin ratio approaches zero. In this

work, the deviation point is defined as the carbon number at the intersection of α_∞ line and the linear regression line of the first three carbon number points (C_4-C_6), as shown in Figure 5.

The observed product distribution, as described above, depends on β (or α_∞) value and olefin to paraffin ratio (f_n) at each carbon number. With some assumptions, the f_n can be simplified to be directly proportional to the vapor pressure. Therefore, with information of reaction temperature, α_∞, and f_3 (depending on reaction condition and catalyst), the dependency of α_n' on carbon number can be simulated and the deviation point can be determined. Table 2 summarized the effect of temperature and f_3 on the deviation point with α_∞=0.9. The effect of α_∞ is insignificant except at high f_3 and high temperature. At 300 ^oC and f_3 = 10 with α_∞=0.8, the deviation point is 15.1, which is merely 1.5 higher than that with α_∞=0.8.

The temperature and f_3 value used in Table 2 pretty much represent the condition and result of a typical FT reaction. It is clear that the VLE model precisely predicts the deviation point to be within carbon number 8-14 which is in agreement with generally experimental observations.

Conclusion

A mathematical model has been developed to describe the product distribution of Fischer-Tropsch synthesis, based on the recognition that the termination path to olefin is reversible. The observed product distribution at the reactor outlet consists of the contribution from intrinsic chain propagation on catalyst surface and the effect of olefin reincorporation. The 2-alpha distribution can be attributed to the effect of vapor liquid separation of hydrocarbon products. The reaction product does not follow ASF single alpha distribution any more even on the catalyst surface. A tight fit between model prediction and experimental data has been demonstrated. Also, the

deviation point of product distribution is precisely predicted to be within carbon number 8-14 under typical FT conditions.

Nomenclature

f	olefin to paraffin ratio
H	vapor liquid equilibrium constant
k_a	olefin adsorption rate constant
k_d	olefin desorption rate constant
k_o	hydrogen abstraction rate constant of chain growth intermediate
k_o'	olefin half hydrogenation rate constant
k_p	propagation rate constant of chain growth intermediate
k_H	hydrogenation rate constant of chain growth intermediate
K_E	reaction equilibrium constant of olefin half hydrogenation ($K_E = k_o/k_o'$)
K_{ad}	adsorption equilibrium constant ($K_{ad} = k_a/k_d$)
L	liquid molar flow rate at reactor outlet
P	total operating pressure
P^s	saturated vapor pressure of hydrocarbon
r	reaction rate
R	gas constant
S	concentration of surface species
T	temperature
V	vapor molar flow rate at reactor outlet
V_R	reactor size (catalyst volume, catalyst weight)
x	molar fraction in liquid phase
y	molar fraction in vapor phase
α	chain propagation probability on surface, a function of carbon number
α'	observed product distribution, a function of carbon number
α_∞	chain propagation probability on surface at high carbon numbers, a constant
λ	factor of olefin reactivity ($\lambda_n = (1+f_n)/(1+f_{n-1})$)
τ	average residence time of hydrocarbon species

subscript

=	olefin
H	hydrogen
n	paraffin, olefin, or chain growth intermediate of carbon number n
o	olefin
p	paraffin

References

1. Zhan, X. and Davis, B.H.; "Two-alpha Fischer-Tropsch product distribution. A role for vapor-liquid-equilibrium?", accepted by Petroleum Science and Technology.
2. Zhan, X. and Davis, B.H.; "Concentration profile of Fischer-Tropsch products in catalyst pores", ACS Petroleum Chemistry prepr., 45(2), 214-217, 2000.
3. Iglesia, E.; "Design, synthesis, and use of cobalt-based Fischer-Tropsch synthesis catalysts", Applied Catalysis A: General, 161 (1997), 59-78.
4. Kuipers, E.W., Vinkenburg, I.H. and Oosterbeek H.; "Chain length dependence of α-olefin readsorption in Fischer-Tropsch synthesis", J. Catalysis, 152 (1995) 137-146.
5. Komaya, T. and Bell, A.T.; "Estimates of rate coefficients for elementary processes occurring during Fischer-Tropsch synthesis over Ru/TiO_2", J. Catalysis, 146 (1994) 237-248.
6. Anderson, R. B., Friedel, H., and Storch, H. H., "Fischer-Tropsch reaction mechanism involving stepwise growth of carbon chain," J. Chem. Phys., 313 (1951) 19.
7. Iglesia, E., Reyes, S.C., and Soled, S.L; "Reaction-transport selectivity models and the design of Fischer-Tropsch catalysts"; in "Computer-Aided Design of Catalysts and Reactors," (E. R. Becker and C. J. Pereira, Eds.), Marcel Dekker, Inc., 1992.

Table1 Two reactions from literature		
	Reaction 1	Reaction 2
Catalyst	Co/TiO_2	Ru/TiO_2
Temperature, ^oC	200	203
Pressure, kPa	2000	560
CO Conversion, %	72	60
α_∞	0.92	0.92
f_3 (olefin/paraffin of C_3)	2.15	3.9
f_4 (olefin/paraffin of C_4)	1.3	2.7

Table 2

Deviation point of alpha value at α_∞=0.9

f_3 / T, ºC	1	5	10
200	8.4	10.6	11.6
250	9.1	11.4	12.5
300	10.0	12.4	13.6

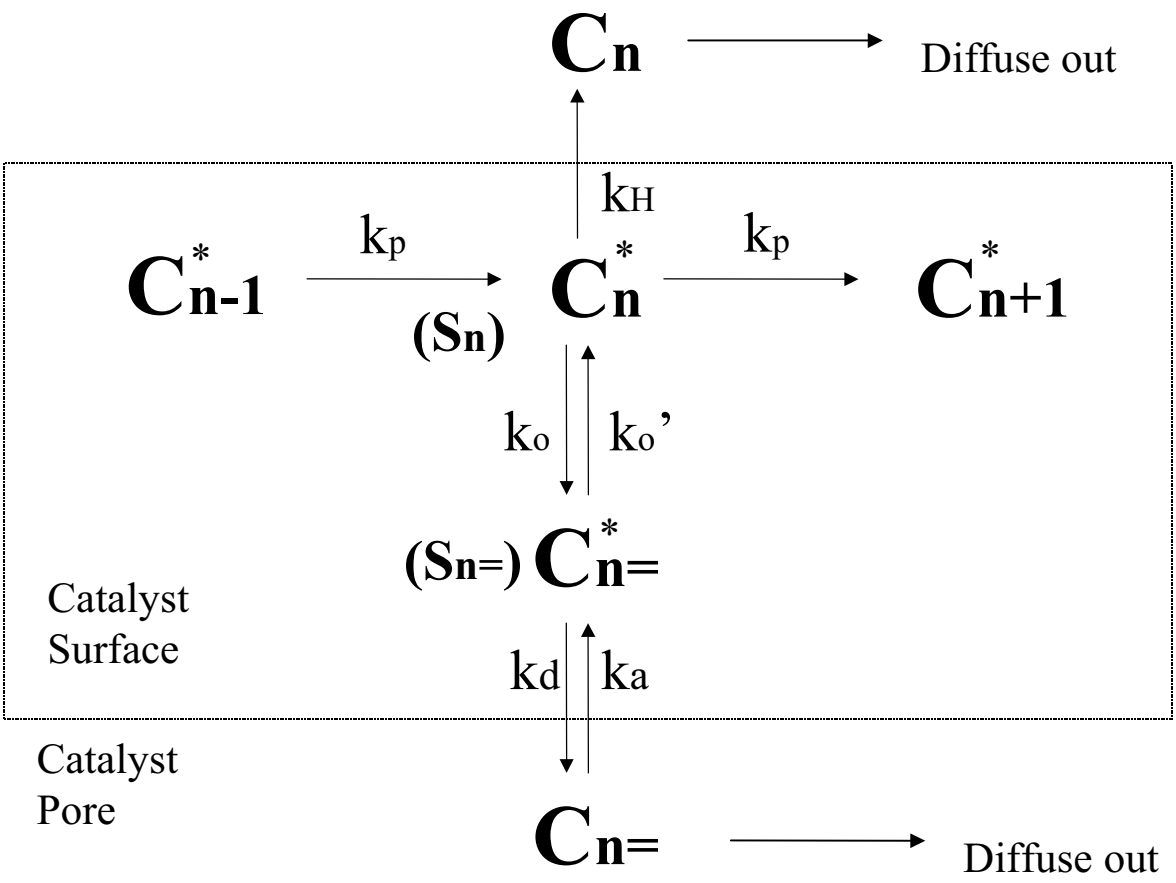

Figure 1 Reaction pathway of Fischer-Tropsch synthesis

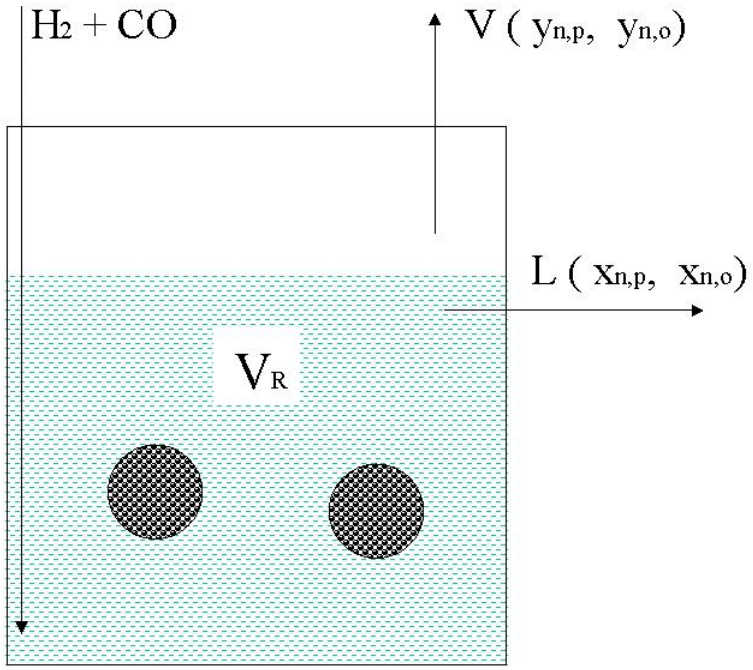

Figure 2 Schematic diagram of a CSTR reactor

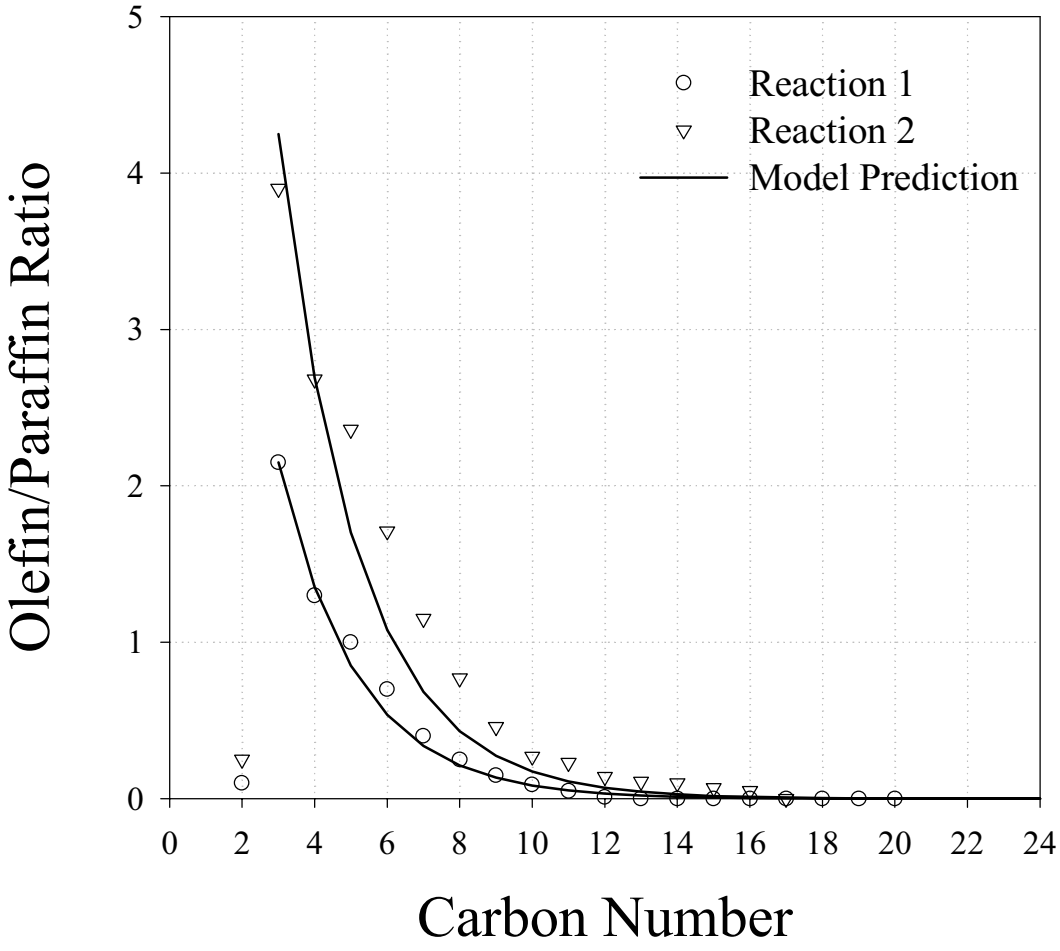

Figure 3 Olefin to paraffin ratio of Model Prediction and Exxon Data

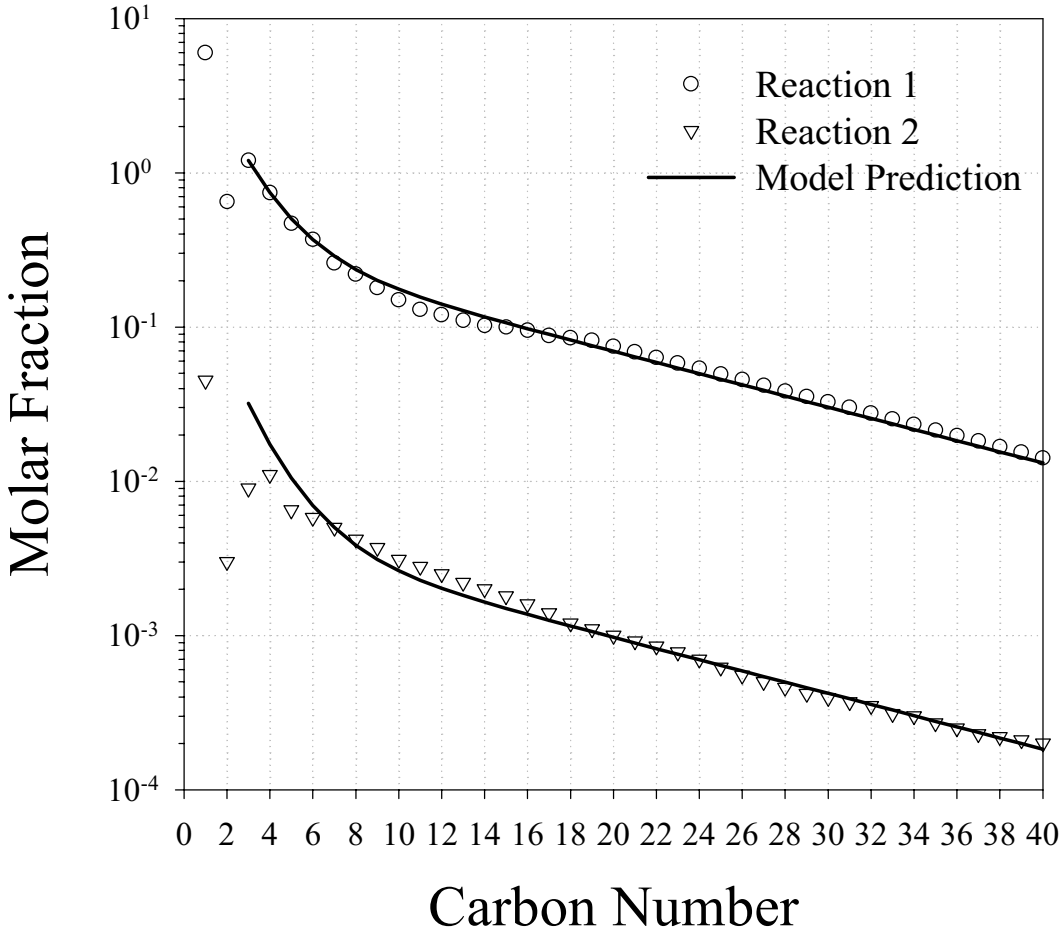

Figure 4 Product distribution of Model Prediction and Exxon Data

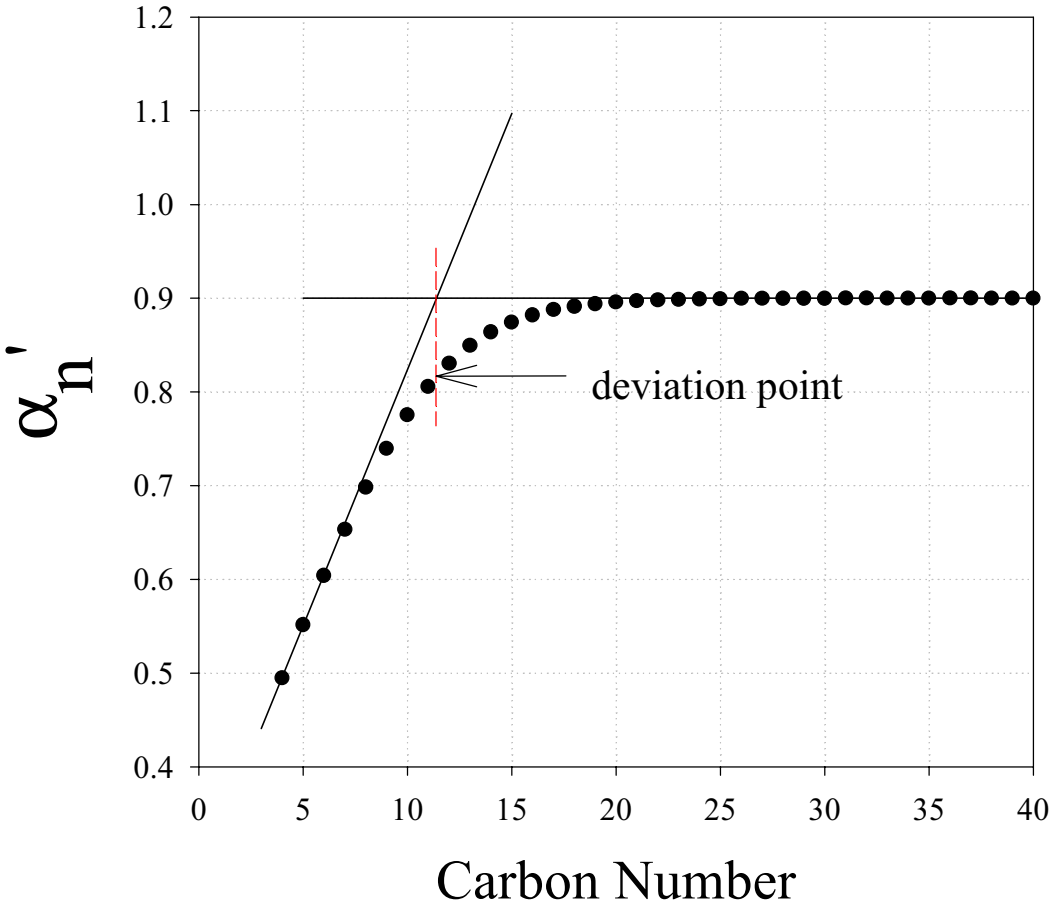

Figure 5 Determination of deviation point
(T=250^{o}C, α_{oo} = 0.9, f_3=5)

B. CO and CO_2 Hydrogenation Over Co/SiO_2 Catalyst

Summary

CO and CO_2 hydrogenation was studied in a fixed bed reactor using a Co/SiO_2 catalyst. The reaction was carried out at 220°C, 350psig, H_2:CO=2:1, H_2:CO_2 = 2.1, with a total flow rate of 150 mL/min (3NL/hr/g catalyst) and a H_2+CO, H_2+CO_2 or H_2+CO+CO_2 flow rate of 50 mL/min(1NL/hr/g catalyst). CO, CO_2 and CO,CO_2 mixture feed gas was used, respectively, for comparison. The results indicated that in the presence of CO, CO_2 hydrogenation was very small. For the cases of only CO or only CO_2 hydrogenation, the activity of the two were similar but the selectivity was very different. For CO hydrogenation, normal Fischer-Tropsch synthesis product distributions were observed with an α of about 0.80; in contrast, the CO_2 hydrogenation product contained about 70% methane. Thus, CO_2 and CO hydrogenation appears to follow different reaction pathways.

Introduction

Fixation of carbon dioxide has become of greater interest in recent years, primarily because of its impact on the environment through the greenhouse effect. One approach that has attracted attention is to produce synthesis gas through its reaction with methane even though the syngas produced only has a H_2/CO ratio of 1 for the idealized reaction. Another option is to recycle carbon dioxide to a gasification unit; however, there is a limit to the amount of carbon dioxide that can be utilized in this manner. Another approach is to hydrogenate carbon dioxide in Fischer-Tropsch synthesis (FTS) plants; this has become an attractive approach even though one must find a source of hydrogen to accomplish this.

For high temperature (330-350°C) FTS the water-gas-shift (WGS) reaction is sufficiently rapid so that it is nearly at the equilibrium composition. The hydrogenation of CO_2 at high

temperatures is possible and occurs in the fluid bed reactors operated by Sasol and Mossgas. However, the use of a slurry phase bubble column reactor is very attractive since its use allows the FTS reaction to be carried out isothermally. In the liquid phase synthesis, lower temperatures must be utilized (220-240ºC) with either a cobalt or iron catalyst. It was of interest to compare the FTS reactions of CO and CO_2 with a cobalt catalyst. In this initial work a simple catalyst formulation has been utilized: cobalt supported on a silica without any promoters.

Experimental

The catalyst was prepared by three incipient wetness impregnations of silica (Davisil 644, 100-200 mesh, 300 m^2/g, and pore volume of 1.15 cm^3/g) with aqueous cobalt nitrate to produce a final loading of 15 wt.% CO. The material was dried in a fluidized bed and then calcined for 4 hrs. in an air flow at 400ºC. Three grams of the calcined catalyst was diluted with 15 g of glass beads and placed in a fixed bed reactor where it was reduced in a H_2(33%)/Ar flow for 10 hours at 350ºC. The reaction conditions were: 220ºC, 24 atm (2.4MPa), H_2/CO = 2/1, 3 NL/hr/g catalyst total gas flow, 1 NL/hr/g catalyst synthesis gas flow. Analysis of the gaseous products was accomplished using gas chromatography.

Results

The conversion of CO and CO_2 during 10 days on-stream are given in figure 1. Compared to the CO conversions of the same and another similar Co-silica catalyst, it appears that the initial CO conversion is about the same in the CSTR and in the fixed bed reactor; however, the activity decline is more rapid in the fixed bed reactor. The run data and conversions for the fixed bed reactor are compiled in table 1.

There was a decline in activity during the period between collecting the first two samples. The exit gas from the CO_2 conversions contained more CO_2 than the calibration gas so that CO_2

conversions were calculated from the mass balance for the other gaseous and liquid products; thus, there is some uncertainty in the absolute CO_2 conversion data but the trend shown in Table 1 and figure 1 is certainly valid. Thus, with the cobalt catalyst the conversion of CO and CO_2 occur at about the same rate. This is in contrast to the observations with an iron catalyst under low temperature FTS conditions where the rate of conversion of CO_2 is considerably lower than for CO (1-6).

A striking difference for the cobalt catalyst is the formation of methane. Under the same reaction conditions, the amount of methane produced is much higher for the CO_2 reactant (figure 2). Whenever CO_2 was the reactant, methane accounted for greater than 70% (based on carbon) of the products. However, under the same reaction conditions and with the same catalyst, methane accounted for less than 10% of the products with CO as reactant. Similar results are reported by Riedel et al. (6). This requires that methane be formed by two pathways or that a common reaction intermediate and reaction pathway does not occur with CO and CO_2.

During period 9, the feed was changes so that equal amounts of CO and CO_2 were present in the feed and the flows of Ar, H_2 and ($CO + CO_2$) were the same as when either pure CO or CO_2 was converted. Under competitive conversions, CO was converted much more rapidly than CO_2, clearly showing that CO is adsorbed on the Co catalyst to a much greater extent than the CO_2. Whereas the total carbon oxide conversion is about the same expected from the trend of the previous runs, the conversion of CO accounted for more than 90% of the total conversion of the carbon oxides. A similar result was obtained following the conversion of methanol except that there was not as dramatic a difference as would be expected from the trend of the previous conversions. The CO conversion following the period of methanol feed was lower than expected from the trend of the prior periods. Since the water partial pressure was much higher during the

conversion of methanol, it is anticipated that irreversible, or slowly reversible, damage of the catalyst occurred during the exposure to the high water partial pressure conditions.

Following the first conversion of the mixture of CO and CO_2, methanol was substituted for the carbon oxides feed. Because of the limitations of the liquid pump, the feed during this period was only H_2 and methanol. The total flow was 4 NL/hr/g catalyst and the H_2/methanol molar ratio was 2/1. Thus, the H2/carbon ratio in the feed was the same as when CO and/or CO_2 was the feed but the flow rate of methanol was four times that of the carbon oxide. Under the reaction conditions used the conversion of methanol was about 50% whereas the conversion of CO or CO_2 was slightly less than 25%. Thus, considering the higher flow rate (4 times higher) and higher conversion (2 times higher) of methanol, the total carbon converted with the methanol feed was about 8 times greater than for the carbon oxides. Thus, the relative rate is rapid enough that any methanol intermediate could be converted to methane so that methanol would not be detected in the liquid sample; unfortunately, in this preliminary run the analysis of the gas sample did not provide a measure of the amount of methanol in the gas phase. The only significant products from the conversion of methanol under the FTS conditions were methane and water; thus, any methanol formed during the reaction could have been converted to methane.

Discussion

The difference in the product distributions obtained from the hydrogenation of CO and CO_2 preclude a common reaction pathway for FTS unless there is a second reaction pathway for the conversion of CO_2, but not CO, to methane. Furthermore, if there is a second pathway, then the FTS with CO_2 occurs at about only 20% of the rate for CO.

Based on the preliminary data, it is proposed that the conversion of CO and CO_2 occurs by different reaction pathways. It is assumed that the hydrogenation and breaking of the two

C-O bonds of the CO_2 provide the source of the different pathways. In this proposal, the breaking of the C-O bond, presumably by the addition of adsorbed H to form C-O-H, competes with, and probably leads, the addition of adsorbed H to form the C-H bond. Thus, for CO the following reaction pathway could apply:

$$C\text{-}O_a + 2\ H_a \rightarrow [\ H - C \text{ --- } O\text{-}H\ ]_a \rightarrow H\text{-}C_a + O\text{-}H_a \qquad [1]$$

In the case of CO_2 the reaction is more complex since there are two C-O bonds that must be broken prior to, or simultaneous with, the formation of the C-H bond. If it is assumed that similar rates apply for the formation of the first O-H and C-H bonds as in the case of CO we would have a different situation, idealized in reaction [2]:

$$O\text{-}C\text{-}O_a + 2\ H_a \rightarrow \begin{array}{c}[\ H - C \text{ --- } O\text{-}H\ ]_a \\ \quad | \\ \quad O\end{array} \rightarrow \begin{array}{c}[H\text{-}C]_a + O\text{-}H_a \\ \quad | \\ \quad O\end{array} \qquad [2]$$

If reaction [2] is valid, it is then a matter of the hydrogenation of the adsorbed oxygen species to produce the adsorbed intermediate (methanol) and its subsequent hydrogenation:

$$[H\text{-}C\text{-}O]_a + 3\ H_a \rightarrow [H_3C\text{-}O\text{-}H]_a + 2\ H_a \rightarrow CH_4 + H_2O \qquad [3]$$

Based on the carbon mass balance, about 75% of the hydrogenation of CO_2 would proceed by reaction [3] and the remainder would involve the breaking of the second C-O bond to continue along the normal FTS reaction pathway that is followed by CO hydrogenation. At this time, while the above mechanism accounts for the products that are produced from the hydrogenation of CO_2, it is very speculative. ^{14}C-tracer studies are planned that should provide some evidence to establish whether the speculation has merit.

The results to date for the hydrogenation of CO_2 indicate that it will not be commercially attractive using typical FTS catalysts based on iron or cobalt.

References

1. L. Xu, S. Bao and B. H. Davis, Role of CO_2 oxygenates and alkenes in the initiation of chain growth during the Fischer-Tropsch synthesis, (M. de Pontes, R. L. Espinoza, C. P. Nicolaides, J. H. Scholz and M. S. Scurell, eds.) Natural Gas Conversion IV (Studies in Surface Science and Catalysis) 107, 175 (1997).
2. L. Xu, S. Bao, D. J. Houpt, S. H. Lambert and B. H. Davis, Role of CO_2 in the initiation of chain growth and alcohol formation during the Fischer-Tropsch Synthesis, Catal. Today, 36, 347 (1997).
3. L. Xu, S. Bao, L-M. Tau, B. Chawla, H. Dabbagh and B. H. Davis, Role of CO_2 in the initiation of chain growth during the Fischer-Tropsch Synthesis, 11th Ann. Int. Pittsburgh Coal Conf. Proc., 88, 1994.
4. L. Xu, S. Bao, L.-M. Tau, B. Chawla, H. Dabbagh and B. H. Davis, Role of CO_2 in the initiation of chain growth during the Fischer-Tropsch synthesis, Preprints ACS Fuel Chem. Div., 40, 153 (1995).
5. L. Xu, S. Bao, L.-M. Tau, B. Chawla, H. Dabbagh and B. H. Davis, Role of CO_2 in the initiation of chain growth during the Fischer-Tropsch synthesis, Proc. 211th National Mtg., ACS, Petrol. Div., 246-248 (1996).
6. T. Riedel, M. Claeys, H. Schulz, G. Schaub, S.-S. Nam, K.-W. Jun, M.-J. Choi, G. Kishan and K.-W. Lee, Comparative study of Fischer-Tropsch synthesis with H_2/CO and H_2/CO_2 syngas using Fe- and Co-based catalysts, Appl. Catal. A: General, 186, 201-213 (1999).

Table 1

Run Conditions and Results from the Conversion of CO and CO_2 with a Cobalt-silica Catalyst

Sample No.	Time on Stream(hrs)	Feed Gas	Conversion(%)
1	17.3	CO	52.2
2	39.47	CO	45.8
3	44.47	CO2	31.2
4	61.97	CO	24.4
5	70.47	CO2	23.1
6	90.97	CO2	20.5
7	109.97	CO	18.6
8	117.22	CO2	24.5
9	134.47	CO+CO2	CO, 53.5% CO2, 3.98%
10		methanol	
11	206.22	CO+CO2(different flow rate)	CO: 9.86% CO2: 6.1%
12	226.89	CO2	22.8

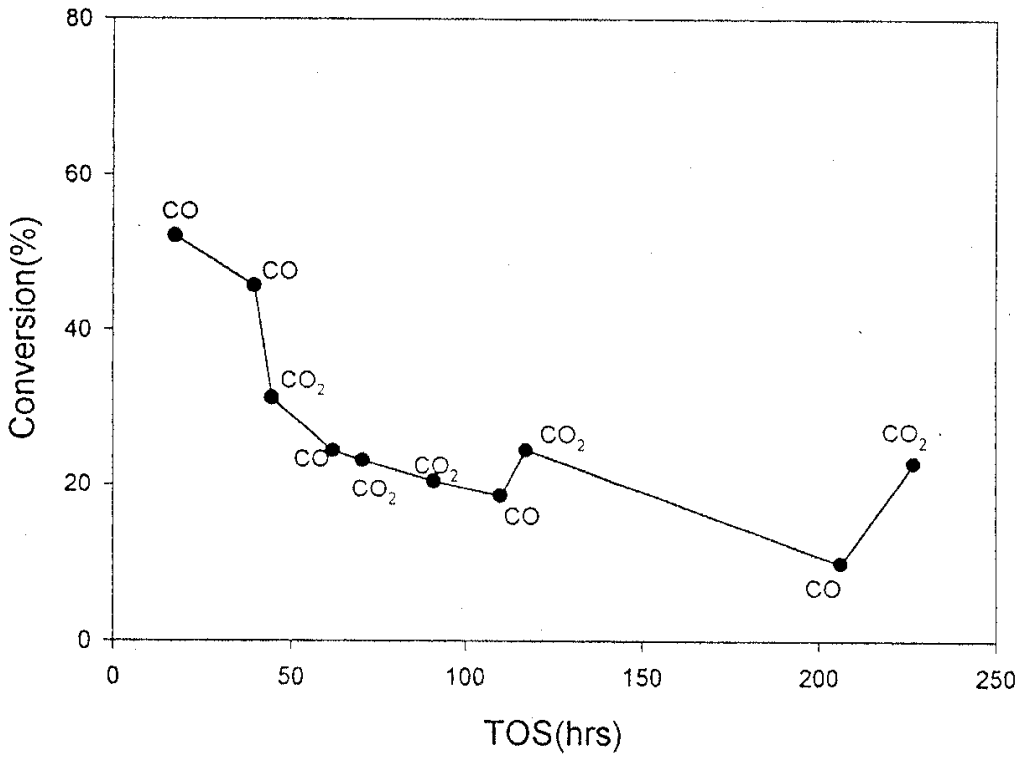

Fig.1 CO and CO_2 conversion as a function of time on stream

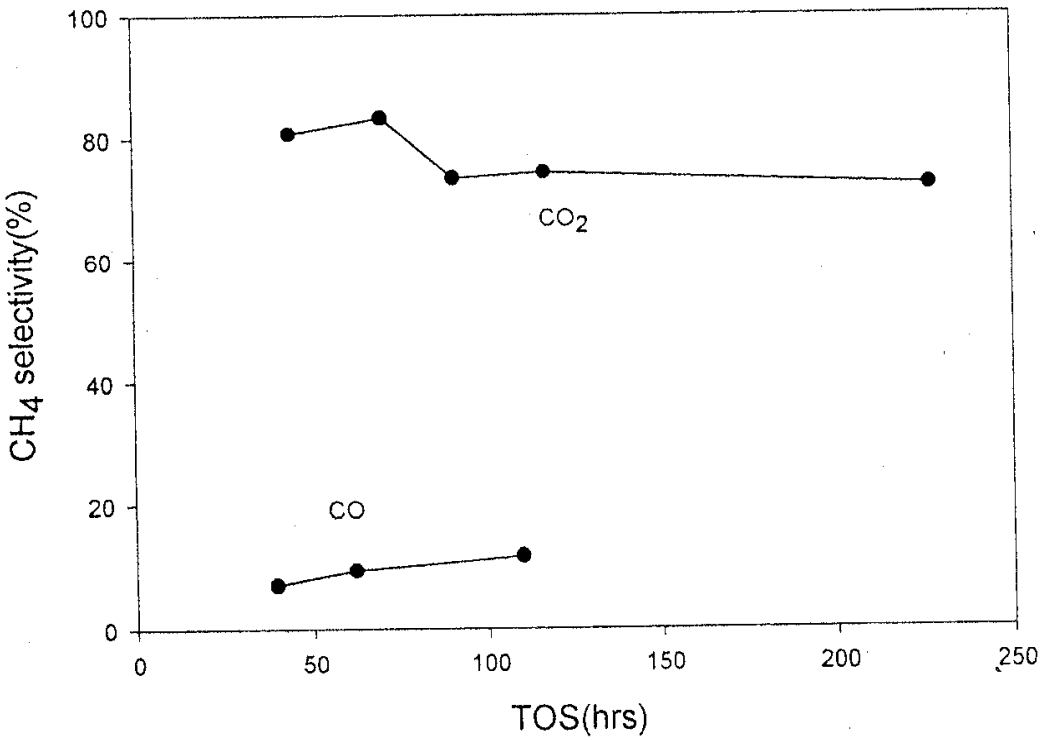

Fig. 2 Methane selectivity as a function of time on stream

Task 11. University of California, Berkeley (Subcontract)

The objective of this task is the characterization of the structure and function of active sites involved in the synthesis of high molecular weight hydrocarbons from CO and H_2 on multi-component catalysts based on Fe as the active component.

Table of Contents

I. FISCHER-TROPSCH SYNTHESIS ON IRON CATALYSTS

1. Background

1.1. Structure and Function of Active Phases in Fischer-Tropsch Synthesis

Fe-based oxides have been used as commercial catalysts for Fischer-Tropsch synthesis (FTS) to produce a wide range of paraffin and olefin products, ranging from methane to high molecular weight waxes [1]. During activation in synthesis gas and subsequent FTS reaction, several phases including metallic iron, iron carbides and iron oxides can co-exist at steady-state conditions [2-5]. The relative amounts of these phases depend on various activation and reaction conditions, which also lead to different catalytic performance. Some researchers [6] have proposed that surface iron atoms are responsible for FTS activity, while others have considered surface carbides or a mixture of carbides [7,8] with metallic iron [9] to be the active phase. There are also some reports that suggest that magnetite Fe_3O_4 is the active FTS phase [10-12]. Although these studies have each provided some evidence to support its specific proposal about the active phase, the available information remains phenomenological and sometimes contradictory, and a direct method to identify the active phase during reaction and to count the number of active sites has remained elusive.

Based on our previous studies of the active phases and catalytic activity on Fe-Zn-K-Cu oxides [23], we have started in this reporting period the preparation of a new series of Ru- and K-promoted Fe-Zn catalysts and investigated the reduction and carburization process and catalytic activity in our search for alternate and superior catalysts for FTS reactions. We also continued our X-ray absorption spectroscopy (XAS) studies on Fe-Zn-Ru-K and Fe-Zn-K-Cu oxides with emphasis on measuring the spectra at FTS conditions (543 K, 5 atm) and with the CO_2 addition in order to simulate the high conversion conditions and to explore any phase changes in these catalysts.

1.2. Effects of Zn, Ru and K on Fe Oxides

Many components have been incorporated into Fe catalysts in order to improve their mechanical and catalytic properties. Our previous studies have shown that Zn, K and Cu [13-15] promote the catalytic properties of Fe oxides. Zinc oxide, as a non-reducible oxide at FTS conditions, appears to stabilize the surface area of Fe oxide precursors. Alkali, as a modifier of the adsorption enthalpies of H_2 and CO, increases the selectivity to the desired C_{5+} products. Copper promotes the carburization processes and decreases the temperature required for the activation of iron oxide precursors. According to our previous optimum composition of Fe-Zn-K-Cu (Zn/Fe=0.1, K/Fe=0.02, Cu/Fe=0.01), we have prepared a series of Zn and Fe co-precipitated oxides with constant Zn/Fe and K/Fe atomic ratios (Zn/Fe=0.1, K/Fe=0.02) and varying amounts of Ru (Ru/Fe=0-0.01). Ru is a very active FTS catalyst. Ru was chosen in order to attempt to improve the catalytic activity and to minimize unfavorable water gas shift reactions that are catalyzed by Cu on Fe catalysts. Also, K was added in order to increase wax and alkene yields, while decreasing the production of undesirable methane products. The same effects of K are

expected on Fe-Zn-Ru-K catalysts. We have examined the surface area, bulk structure, required reduction and carburization temperatures, as well as the catalytic behavior of these catalysts, in order to identify optimum Ru contents that give maximum site density and catalytic activity.

2. Synthesis Procedures

2.1 Fe-Zn-K-Cu Oxides

Fe-Zn-K-Cu catalysts were prepared by co-precipitation of iron and zinc nitrates followed by the impregnation of an aqueous solution of potassium carbonate and copper nitrate using incipient wetness methods. The detailed preparation procedure was described in our previous report [18].

2.2. Fe-Zn-Ru-K Oxides

All catalysts were prepared by co-precipitation of iron and zinc nitrates (Aldrich, 99+%) at a constant pH of 7.0 in order to form porous mixed oxides. Then, these oxide precursors were impregnated with a ruthenium (III) nitrosyl nitrate [$Ru(NO)(NO_3)_x(OH)_y$ (x+y=3)] (Aldrich, solution in dilute nitric acid, Ru 1.5%) and with an aqueous solution of potassium carbonate (Aldrich, 99+%) and copper nitrate (Aldrich, 99+%) using incipient wetness methods. The Zn/Fe oxide precursors were prepared first. Fe nitrate (1.4 M) and Zn nitrate (3.0 M) solutions were mixed at a given Zn/Fe atomic ratio (Zn/Fe=0.1). A solution of ammonium carbonate (Aldrich, 98%) (1 M) was prepared separately. Deionized water (~ 50 ml) was added into a large flask, which was heated on a hot plate with a magnetic stirrer and held at 353 K throughout the synthesis. The mixed Zn/Fe solution was added at 2 cm^3/min flow into the flask using a rotary pump. At the same time, the ammonium carbonate solution was fed separately, and its flow was controlled to maintain the slurry pH at 7±0.1, as monitored by a pH meter. The resulting precipitates (~20 g) were washed several times with about 1 *l* water per gram of catalyst, dried at 393 K overnight, and then treated in dry air at 623 K for 1 h. The air-treated material was promoted with a ruthenium (III) nitrosyl nitrate [$Ru(NO)(NO_3)_x(OH)_y$ (x+y=3)] (Aldrich, solution in dilute nitric acid, Ru 1.5%) using incipient wetness protocols and then dried at 373 K. The dried material was treated in dry air at 623 K for 4 h. A similar process was used in order to promote samples with 2 at.% K using a K_2CO_3 solution (0.16 M). Finally, the dried material was treated again in dry air at 623 K for 4 h. These catalysts were pressed into pellets at 440 MPa, lightly crushed, and then sieved in order to retain the 80-140 mesh (100~180 μm) fraction used for FTS reactions and for all subsequent characterization studies.

3. Catalyst Characterization

3.1. Protocols for the Characterization of Fe-based FTS Catalysts

This research program addresses the synthesis and the structural and catalytic characterization of active sites in Fe-based catalysts for FTS. We have designed a matrix

of samples consisting of a systematic range of multicomponent catalysts in order to determine the number and type of surface sites present on fresh catalysts and on samples during and after FTS reaction (Table 1.1). Our objective is to develop rigorous relationships between the synthesis methods, the resulting catalyst structures, and their function in FTS reactions.

3.2. BET Surface Area

The surface area measurements were conducted on the Fe-Zn-Ru-K samples using the BET method (Table 2). Fe-Zn precursors (Zn/Fe=0.1) prepared by a co-precipitation method and subsequent treatment in air at 623 K have a surface area of 115 m^2g^{-1}, which is slightly higher than that of pure Fe_2O_3 (101 m^2g^{-1}) [18] due to the structural promotion effect of Zn. In order to increase the surface area of catalysts, we chose 623 K to treat the Ru and K promoted Fe-Zn samples instead of 673 K, which is the temperature we used to treat Fe-Zn-K-Cu oxides, because ruthenium (III) nitrosyl nitrate decomposes below 623 K. The addition of less than 1 at. % Ru (Ru/Fe ratio = 0.005, 0.01) did not influence the surface area of Fe-Zn oxides (115 vs 108 m^2g^{-1}). Further impregnation of K (K/Fe=0.02) slightly decreased the surface area of Fe-Zn-Ru oxides (Table 2). Compared with a Fe-Zn-K-Cu oxide sample (Zn/Fe=0.1, K/Fe=0.02, and Cu/Fe=0.01) treated at 673 K with a surface area of 65 m^2g^{-1} [18], the Fe-Zn-Ru-K sample showed ~40% higher surface area than Fe-Zn-K-Cu oxides by lowering the treatment temperature by 50 K. Therefore, for the Fe-Zn based catalysts, the treatment temperature strongly influences their surface areas. Impregnation of promoters (Cu, Ru, Re, K etc.) and the length of treatment time (1-4 h) have little effect on the surface area of the catalysts.

Table 2. Surface areas (m^2g^{-1}) of Fe-Zn-Ru-K (Zn/Fe=0.1) samples

Fe-Zn	Fe-Zn-Ru0.5	Fe-Zn-Ru1	Fe-Zn-Ru0.5-K2	Fe-Zn-Ru1-K2
115	115	108	97	90

3.3 In-situ X-ray Absorption (XAS) Measurements of Structural Evolution in FTS

During this reporting period, we have continued our X-ray absorption studies at the Stanford Synchrotron Radiation Laboratory (SSRL) with emphasis on measuring the spectra at FTS conditions (543 K, 5 atm) and with the CO_2 addition to the synthesis gas stream in order to simulate high conversion conditions and to examine any phase change in these catalysts. We have started the *in-situ* X-ray absorption studies of the structural evolution during initial and long-term FTS reaction on Fe-Zn-Ru-K oxides. The experimental methods have been described in previous quarterly reports [22].

Table 1.1. Matrix of samples and characterization methods for FTS reaction

Nominal Composition of the Catalysts			Characterization Before and After FTS	FTS reaction
Zn/Fe mole ratio	K/Fe (at.%)	Cu/Fe (at.%)		
0	0	0	XRD Surface area In-situ XAS H_2-TPR CO-TPR	Effect of reaction condition 220 °C 21.4 atm 235 °C 21.4 atm 270 °C 5 atm Effect of CO_2 addition Isotopic studies
		1		
	2	0		
		1		
		2		
	4	1		
0.05	0	0		
	2	1		
	4	2		
0.1	0	0		
		1		
	2	0		
		1		
		2		
	4	1		
0.2	0	0		
	2	1		
	4	2		
0.4	0	0		
		1		
	2	0		
		1		
		2		
	6	1		
Zn/Fe	Ru/Fe (at.%)	K/Fe (at.%)		
0.1	0.5	0		
	1			
	0.5	2		
	1			

Figure 1.1a shows the structural evolution of Fe-Zn-Ru1-K2 oxide with time on stream during FTS at 523 K. The spectra are accurately described by a linear combination of the X-ray absorption near edge spectroscopy (XANES) of standard Fe_2O_3, Fe_3O_4, and θ-Fe_3C compounds. These data showed that Fe_2O_3 was readily converted to Fe_3O_4 and Fe carbides after exposure to synthesis gas (<1 h). The concentration of Fe_3O_4 decreased significantly as a function of time on stream while the concentration of θ-Fe_3C increased monotonically as the FTS reaction proceeded. After 4 h on stream, Fe_3O_4 was completely converted to θ-Fe_3C. Compared with our previous studies on Fe_2O_3 [20], the addition of Ru and K to Fe-Zn oxides significantly increases the reduction and carburization of Fe oxides. Increasing reaction temperature up to 543 K, the concentration of Fe carbide does not change, and thus the results are not presented here.

Thermodynamic calculations (1) showed that the reaction of Fe carbides with CO_2 at 543 K and at 1 atm requires a CO_2/CO ratio larger than 13.0. XAS results confirmed that the addition of CO_2 to the synthesis gas stream with a CO_2/CO ratio of 6 does not change the concentration of initially formed Fe carbides (Figure 1.1b). When increasing the CO_2/CO ratio up to 14, which is slightly larger than the equilibrium CO_2/CO ratio, the concentration of Fe_3O_4 increases while that of θ-Fe_3C decreases (Figure 1.1c), indicating the oxidation of Fe carbides in the presence of CO_2. However, this oxidation process is slow at the conditions investigated. In order to get a more evident CO_2 addition effect within the limited beam time, we increased the CO_2/CO ratio up to 58 (Figure 1.1c), which is far beyond the equilibrium CO_2/CO ratio, the concentration of Fe_3O_4 and θ-Fe_3C phases changes markedly with the concentration of Fe_3O_4 going up to ~80 % and that of θ-Fe_3C decreasing down to 20 % within 2.5 h. Fe_2O_3 or other Fe oxides were not observed throughout the CO_2 addition process, reflecting the thermodynamically unfavorable oxidation of Fe_3O_4 with CO_2. When removing CO_2 from the synthesis gas, the concentration of Fe_3O_4 and Fe carbide begins to approach to their previous concentrations in pure synthesis gas. All these observations indicate that the stability of Fe oxide or carbide phases is determined by the CO_2/CO ratio. The oxidation of Fe carbides requires a large CO_2/CO ratio (>13) at 543 K and at 1 atm in synthesis gas. At high-pressure FTS conditions (20-30 atm), it is expected to require even larger CO_2/CO ratio.

$$Fe_3C + 5\ CO_2 \rightleftharpoons Fe_3O_4 + 6CO \qquad \Delta G^0_{543K} = 70.45\ kJ/mol \qquad (1)$$

3.4. Reduction of Fe-Zn-Ru-K Oxides in H_2

The Fe-Zn-Ru-K oxides show similar reduction profiles as Fe_2O_3. i.e., Fe_2O_3 is first reduced to Fe_3O_4 and then to metallic Fe (Figure 1.2). The Fe-Zn oxide reduction peaks occur at 325 K and 495 K, respectively. The area (amount of oxygen removed) under the first and second reduction peaks is ~1:10, slightly lower than the 1:8 ratio expected from Fe_2O_3 reduction to Fe_3O_4 and then to Fe. This is because of the presence of $ZnFe_2O_4$, which reduces to Fe_3O_4 and ZnO within the temperature range of the Fe_3O_4 reduction. Those portions of Fe_2O_3 that combined with ZnO reduce at higher temperatures (>650 K).

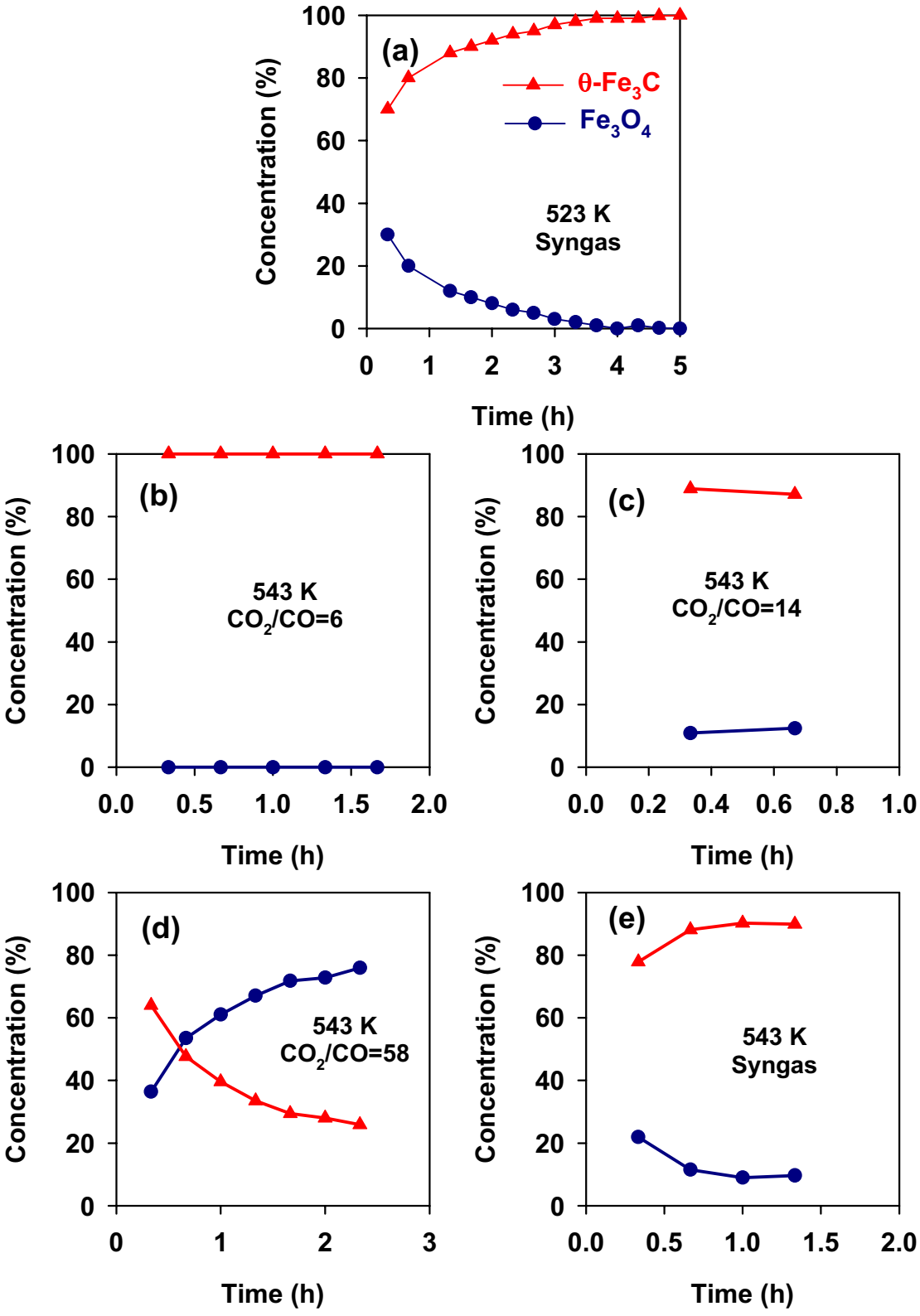

Figure 1.1 *In-situ* XAS phase compositions with CO_2 addition (1 mg sample, Zn/Fe=0.1, Ru/Fe=0.01, K/Fe=0.02) as a function of time in synthesis gas (H_2/CO=2, Synthesis gas flow rate= 30000 cm^3/g-h) at 543 K.

The addition of 0.5 at.% Ru to Fe-Zn oxide decreases the reduction temperature by ~130 K relative to that on Fe-Zn oxide; this appears to reflect the H_2 dissociation sites provided by the Ru component. Consequently, the reduction from Fe_3O_4 to Fe initiates at lower temperatures than on samples without Ru. Increasing Ru addition amount up to 1 at.%, the reduction temperature for Fe_2O_3 conversion to Fe_3O_4 decreases slightly (~5 K); the reduction rate from Fe_3O_4 to Fe, however, increases markedly and the peak temperature decreases by ~35 K. Adding 2 at.% K Fe-Zn-Ru0.5 (Ru/Fe=0.005) sample inhibits the reduction of Fe_2O_3, as indicated by the increased reduction temperature (~30 K). K addition does not appear to influence the reduction of Fe-Zn-Ru1 (Ru/Fe=0.01) sample, whose effect is apparently overshadowed by the strong promotion effect of Ru. Overall, the addition of Ru significantly decreased Fe_2O_3 reduction temperatures and increased Fe_3O_4 reduction rates in H_2. K slightly inhibited Fe oxide reduction. But its inhibiting effect was not evident in the presence of Ru.

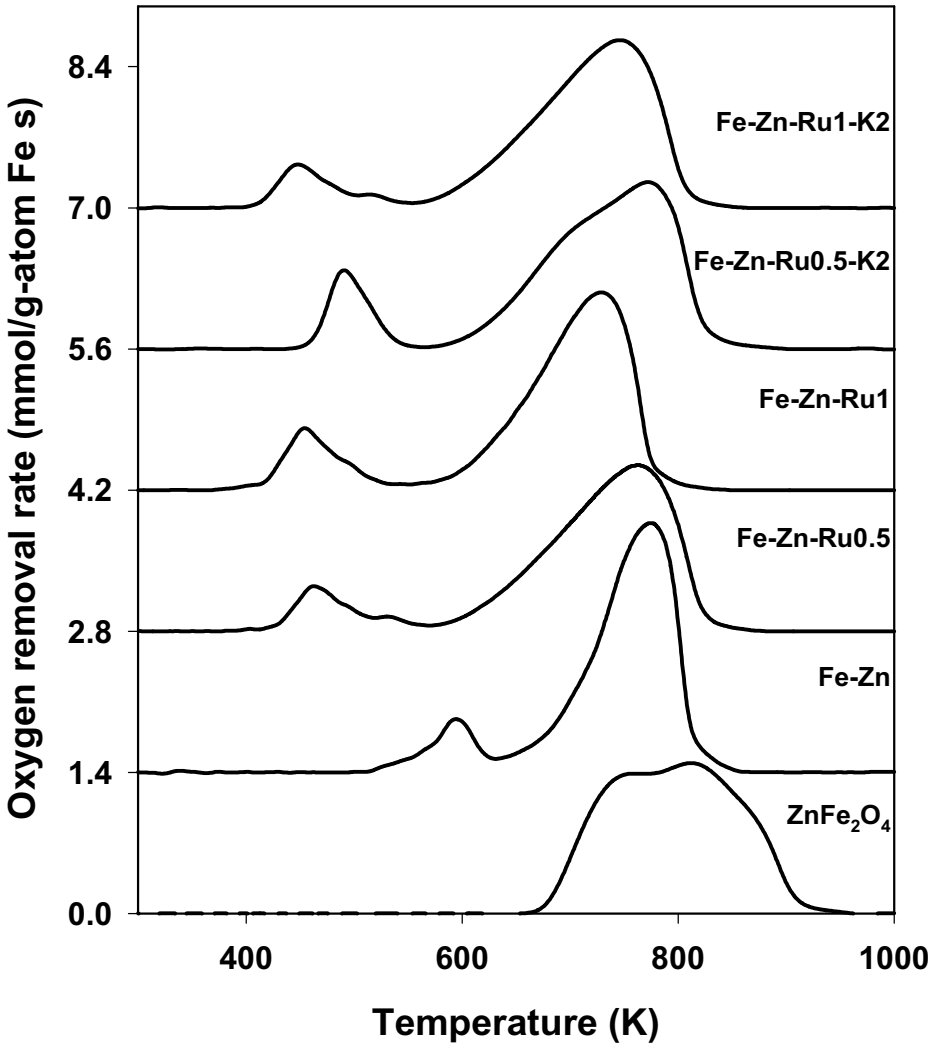

Figure 1.2. TPR of Fe-Zn-Ru-K samples in H_2. (0.2 g samples; 10 K/min ramping rate; Zn/Fe=0.1, K/Fe=0.02, Ru/Fe=0-0.01; 100 cm^3/min, 20% H_2/Ar.)

3.5. Reduction and Carburization of Fe-Zn-Ru-K Oxides in CO

Temperature-programmed reduction and carburization of Fe-Zn-Ru-K oxides in CO were also carried out. A typical TPSR of Fe-Zn-Ru-K oxides (Figure 1.3a) in CO follows a reduction/carburization profile similar to that for Fe_2O_3. Generally, the reduction and carburization of the oxides proceeds in three steps: Fe-Zn oxide is first reduced to Fe_3O_4 (450-550 K); Then, Fe_3O_4 is reduced to metallic Fe followed by carburization to Fe carbides (550-700 K). Excess free carbon forms at higher temperature (>700 K) via the Boudouard reaction. Figure 1.3b shows the reduction/carburization of $ZnFe_2O_4$ in CO. The reduction and carburization occur at much higher temperatures (~200 K) on $ZnFe_2O_4$ than on Fe_2O_3. Also the reduction and carburization peaks of $ZnFe_2O_4$ overlaps because of the high reduction temperatures. $ZnFe_2O_4$ is readily carburized as soon as it is reduced.

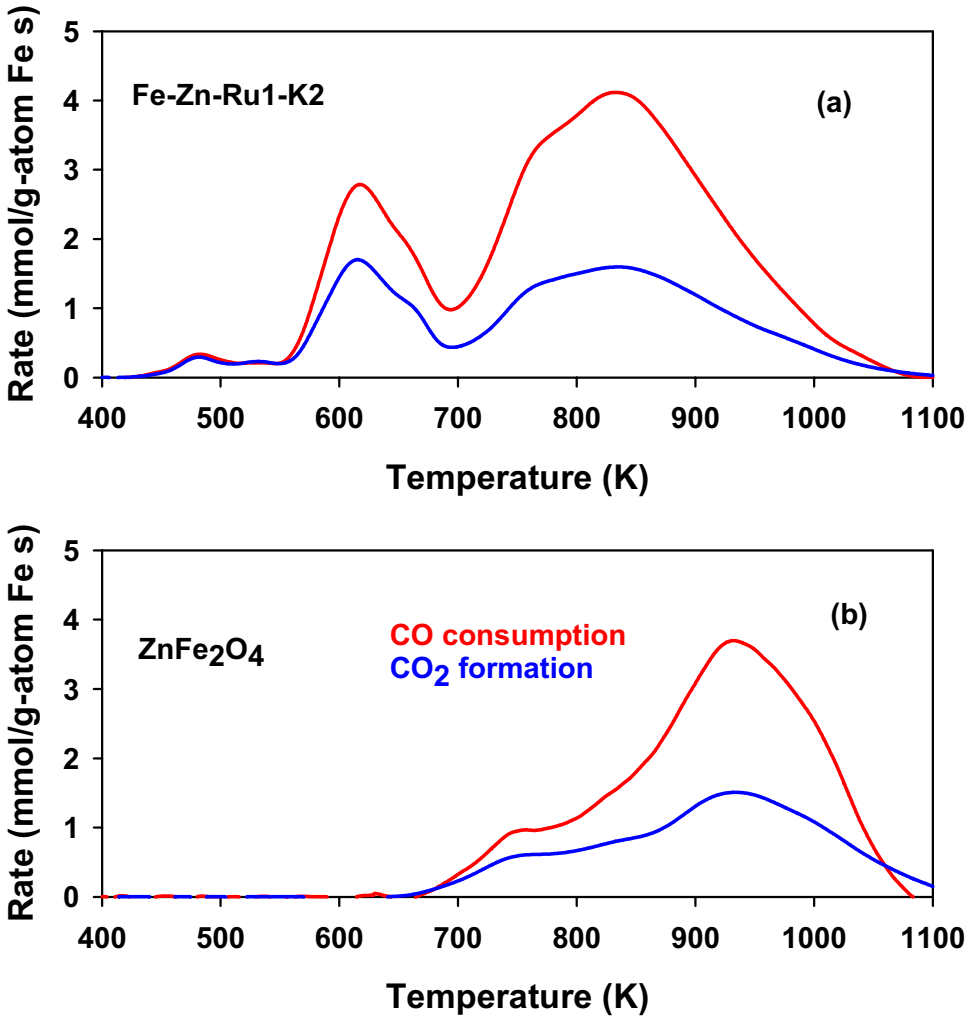

Figure 1.3 The reduction and carburization of (a) $ZnFe_2O_4$ and (b) Fe-Zn-Ru-K oxides in CO (0.2 g samples; Zn/Fe=0.1, K/Fe=0.02, Ru/Fe=0.01; 10 K/min ramping rate; 100 cm^3/min, 20% CO/Ar).

Figure 1.4 shows the reduction and carburization rate of Fe-Zn-Ru-K oxides in CO as a function of temperature. Fe-Zn oxides reduce and carburize at 50-80 K lower temperatures than Fe_2O_3. This is probably because that $ZnFe_2O_4$, which has the same spinel structure as that of Fe_3O_4, acts as nuclei that increase the conversion from Fe_2O_3 to Fe_3O_4. It appears that $ZnFe_2O_4$ as a structural promoter increases the reduction and carburization of Fe oxides in CO. Compared with the reduction/carburization of Fe_2O_3, $ZnFe_2O_4$ in Fe-Zn oxides appears to act also as nuclei for the Boudouard reaction. The carbon deposition is significantly higher on Zn-containing samples than on Zn-free samples. The addition of Ru (Ru/Fe=0.005-0.1) evidently decreases the temperature (~50 K) required to reduce and carburize Fe-Zn oxides using CO. This is apparently because Ru increases CO chemisorption and dissociation rates. Adding K to Fe-Zn-Ru oxides slightly inhibits the reduction from Fe_2O_3 to Fe_3O_4, but on the other hand, it slightly increases carburization rates. Apparently the electron donation effect of K to Fe accounts for the inhibited reduction and favorable CO dissociation. This is in agreement with our previous studies of K effect on the reduction/carburization of Fe-Zn-Cu oxides in CO (19). As a conclusion, Ru increases Fe-Zn oxide reduction and carburization in CO, combined with the contribution from K, a favorable FTS activity can be expected from Ru- and K-promoted Fe-Zn catalyst.

3.5. Effects of Treatment Temperature on Reduction/Carburization of Fe-Zn-Ru-K Oxides in H_2 and CO

Since Ru oxides have high vapor pressures at low temperatures, the treatment temperature plays a critical role in dispersing Ru oxides on Fe oxide. As a consequence, thermal treatments may sensitively influence the reduction and carburization properties as well as the FTS activity of Ru-containing samples. Therefore, it is necessary to find out an optimum treatment temperature in order to maximize Ru dispersion. In addition to the usual treatment temperature 623 K, we also tried a lower temperature (523 K). We prepared a co-precipitated Fe-Zn oxide precursor. After treatment at 623 K for 1 h as usual, we promoted with Ru (Ru/Fe=0.005) and treated in dry air at 523 K or at 623 K for 4 h, respectively. Figure 1.5 shows the effect of treatment temperature on the reduction and carburization of Fe-Zn-Ru0.5 oxide in H_2 and CO. The sample treated at 523 K requires slightly lower reduction temperatures than that treated at 623 K for the reduction of Fe_2O_3 to Fe_3O_4 in H_2. The effect is more evident on the reduction from Fe_3O_4 to Fe, for which the required reduction temperature decreases by ~40 K. The treatment temperature does not appear to influence the reduction and carburization of Fe-Zn oxide in CO as evident as that in H_2 although lower treatment temperatures slightly increase its reduction and carburization rates in CO.

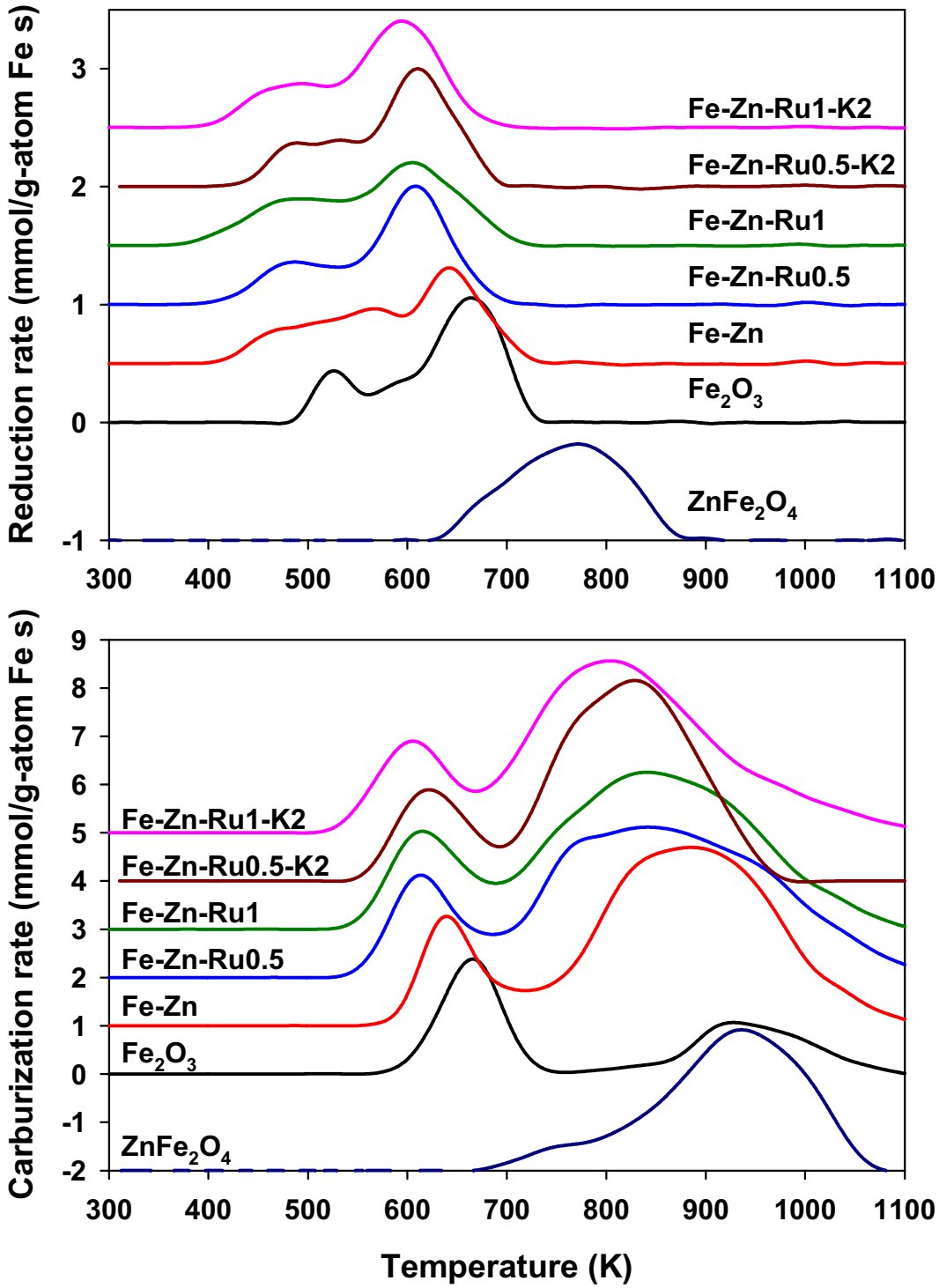

Figure 1.4 The reduction and carburization of Fe-Zn-Ru-K oxides in CO (0.2 g samples; Zn/Fe=0.1, K/Fe=0.02, Ru/Fe=0-0.01, 10 K/min ramping rate; 100 cm^3/min, 20% CO/Ar).

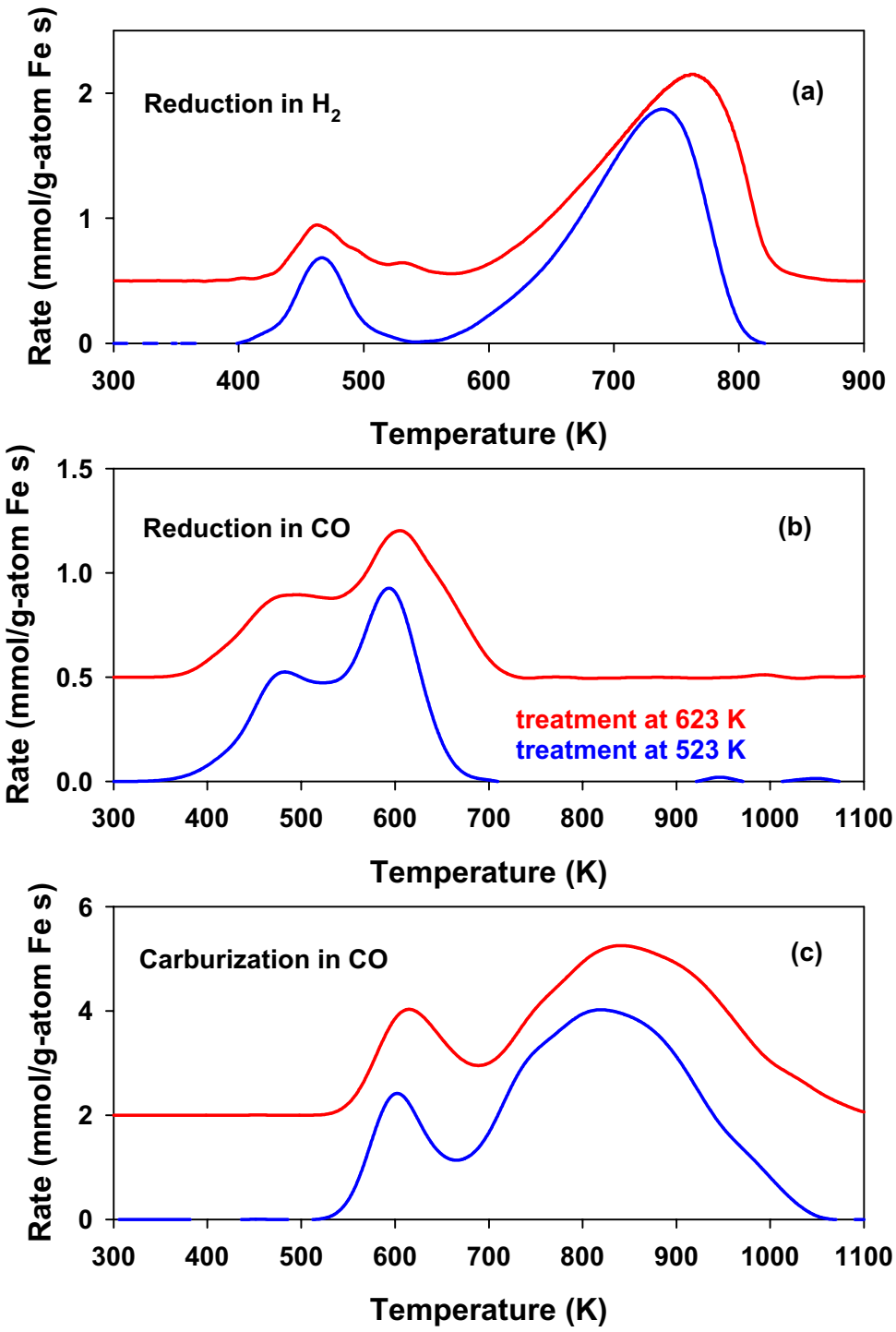

Figure 1.5 The reduction and carburization of Fe-Zn-Ru oxides in H_2 and in CO (0.2 g samples; Zn/Fe=0.1, Ru/Fe=0.005, 10 K/min ramping rate; 100 cm^3/min, 20% H_2 or CO in Ar).

3.6. Isothermal Switch Transient Studies of Fe-Zn-Ru-K Oxides in Synthesis Gas

During the last reporting period, we investigated Re- and K-promoted Fe-Si oxide catalyst. A comparison between the FTS reaction rates on Fe-Si-K and Fe-Zn-Cu-K catalysts showed that the Fe-Si-based catalyst has a higher FTS activity. However, the Fe-Zn-Cu-K catalyst had a higher selectivity to C_{5+} hydrocarbons and a lower CH_4 selectivity under the same conditions. The addition of K or Re promoters did not show significant effects on the reduction/carburization and FTS activity because a large fraction of the K added titrates the SiO_2 component and also because ReO_x was not completely reduced to Re metal during FTS. Therefore, in this reporting period, we moved our focus back to Fe-Zn precursors and promoted them with K and Ru in order to improve their catalytic properties.

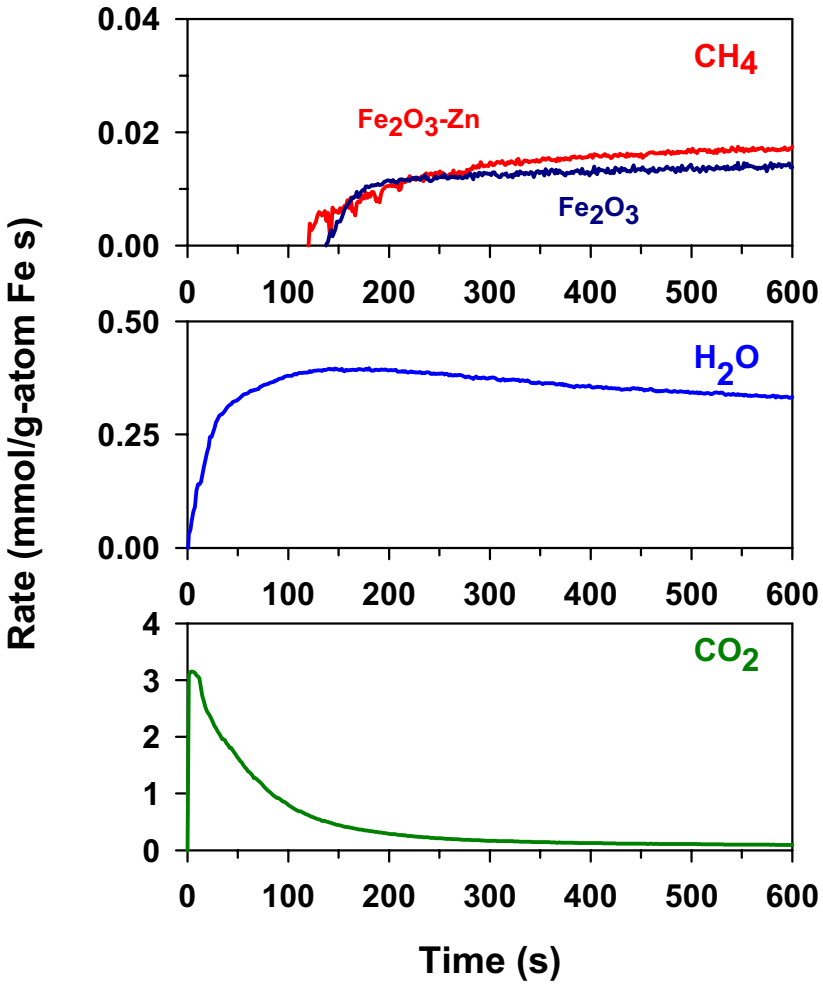

Figure 1.6 Comparison of isothermal product transients of Fe_2O_3 and Fe-Zn oxide (0.2g, Zn/Fe=0.1) in synthesis gas (H_2/CO=2, 60 % synthesis gas in Ar, total flow rate 100 cm^3/min) at 523 K.

A rapid switch transient method with mass spectrometric analysis was used in order to determine the initial reduction and carburization behavior of Fe oxides, as well as their catalytic CO hydrogenation properties in H_2/CO mixtures. Typically, samples (0.2 g) were pretreated in dry air (100 cm^3/min) at temperatures up to 573 K and cooled down in He to 523 K. The He stream was switched to a flow of 60 % synthesis gas (H_2/CO=2) in Ar (total flow rate 100 cm^3/min) at 523 K. The resulting isothermal transients of CH_4, H_2O, and CO_2 products were monitored as a function of time using on-line mass spectrometry and matrix deconvolution methods.

Figure 1.6 shows the isothermal transients measured at 523 K during reduction and carburization and subsequent FTS of Fe-Zn oxide in synthesis gas (H_2/CO=2). Fe-Zn oxide shows similar initial product transient patterns as Fe_2O_3 except that the induction period is slightly shortened and the CH_4 formation rate is slightly higher. CO is the preferential reductant for Fe-Zn oxide in H_2/CO mixtures as evidenced by the large CO_2/H_2O ratio in reaction products. The higher surface area of Fe-Zn oxide appears to be responsible for the higher FTS rates obtained on Fe-Zn oxide precursors compared with Fe_2O_3.

Figure 1.7 shows the isothermal transients measured at 523 K during reduction and carburization and subsequent FTS of Fe-Zn-Ru0.5 oxide in synthesis gas (H_2/CO=2). Fe-Zn-Ru0.5 oxide shows slightly different initial product transients than that of Fe-Zn oxide. Not only is the induction period slightly shortened, but also CH_4 formation rates continue to increase slightly with time on stream. CH_4 formation rates increase by ~50% between 0.1 h and 1 h (Figure 1.7b).

Compared with Cu-promoted Fe oxides [22], for which CuO reduction peaks can be observed after exposure to synthesis gas, there is no appreciable Ru oxide reduction peaks in spite of its immediate reduction, indicated by the instant formation of H_2O and CO_2. This suggests that Ru oxide reduction is not as fast as that of CuO. However, compared with Fe-Zn oxides, the larger amount of oxygen removed during the induction period and the continuous increase in CH_4 formation rates on Ru containing samples suggest that Ru oxides or Ru increases Fe oxide reduction and increases the formation rate of Fe carbides and the evolution of active Fe carbide structures with time on stream.

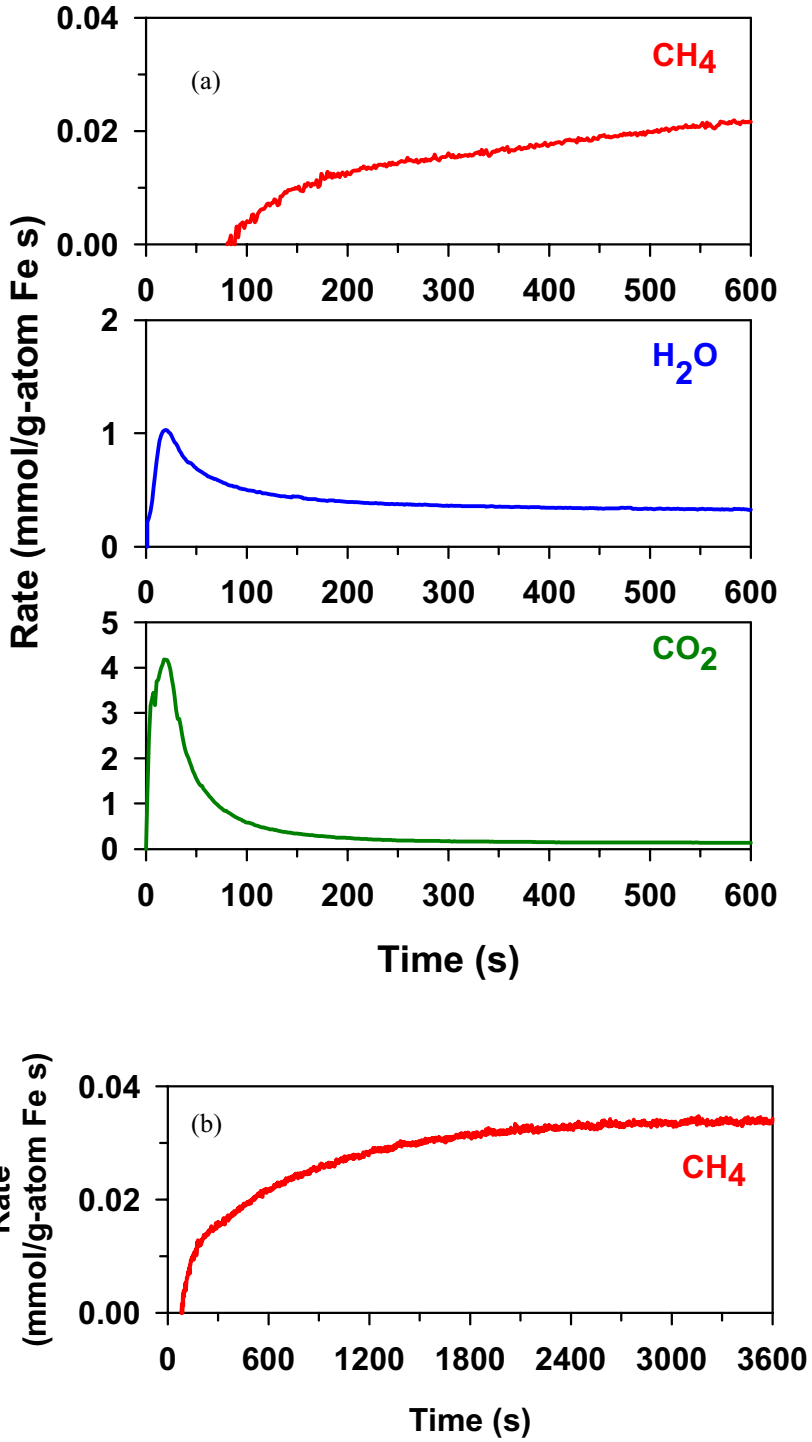

Figure 1.7 Isothermal product transients of Fe-Zn-Ru0.5 oxide (0.2g, Zn/Fe=0.1, Ru/Fe=0.005) in synthesis gas (H_2/CO=2, 60 % synthesis gas in Ar, total flow rate 100 cm^3/min) at 523 K.

Figure 1.8 shows the isothermal transients measured at 523 K during reduction and carburization and subsequent FTS of Fe-Zn-Ru1 oxide in synthesis gas (H_2/CO=2). Fe-Zn-Ru1 sample shows almost same FTS profile to Fe-Zn-Ru0.5 sample oxide except the induction period is even shorter and the oxygen removed (via H_2O and CO_2) is about ~2 times larger than on the Fe-Zn-Ru0.5 sample. Therefore, the effect of Ru oxides or Ru is to increase reduction rates and assist in the evolution of active Fe carbides. Since Ru itself is a very active FTS catalyst, reduced Ru can also contribute to the increased CH_4 formation rates.

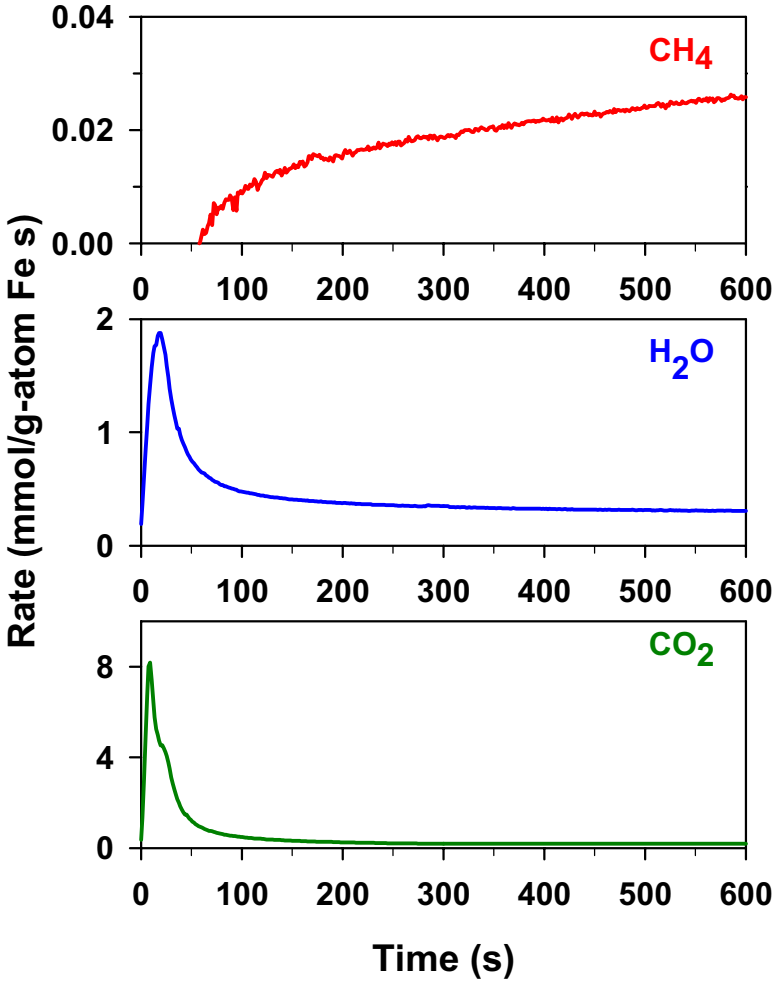

Figure 1.8 The isothermal product transients of Fe-Zn-Ru1oxide (0.2g, Zn/Fe=0.1, Ru/Fe=0.01) in synthesis gas (H_2/CO=2, 60 % synthesis gas in Ar, total flow rate 100 cm^3/min) at 523 K.

Figures 1.9 and 1.10 show the isothermal transients measured at 523 K during reduction and carburization and subsequent FTS of Fe-Zn-Ru0.5-K2 and Fe-Zn-Ru1-K2 oxide in synthesis gas (H_2/CO=2), respectively. Apparently the addition to Fe-Zn-Ru oxide slightly inhibits the reduction as indicated by the lower amount of oxygen removed during the induction period on the K-containing samples. However, the induction period is shortened compared with Fe-Zn-Ru samples without K. CH_4 formation rates increase initially and rapidly reach a relatively stable value. There is no appreciable change of CH_4 formation after 1 h reaction. Therefore, K appears to increase carburization rates and to stabilize the active surface Fe carbide species.

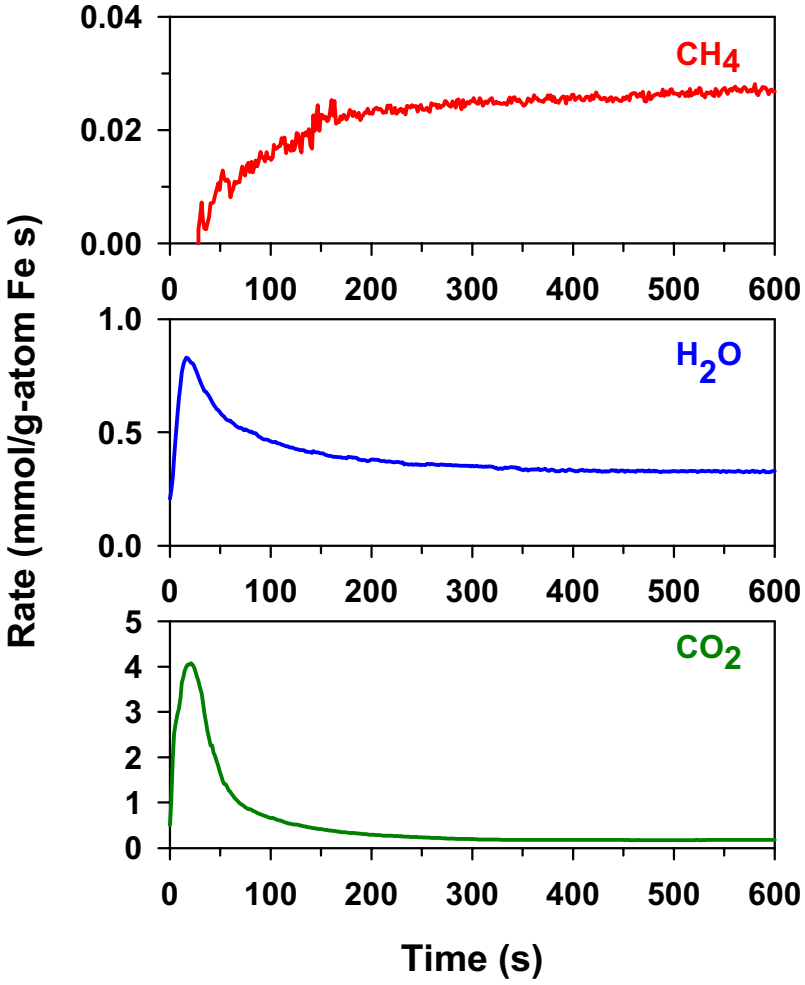

Figure 1.9 Isothermal product transients of Fe-Zn-Ru0.5-K2 oxide (0.2g, Zn/Fe=0.1, Ru/Fe=0.005, K/Fe=0.02) in synthesis gas (H_2/CO=2, 60 % synthesis gas in Ar, total flow rate 100 cm^3/min) at 523 K.

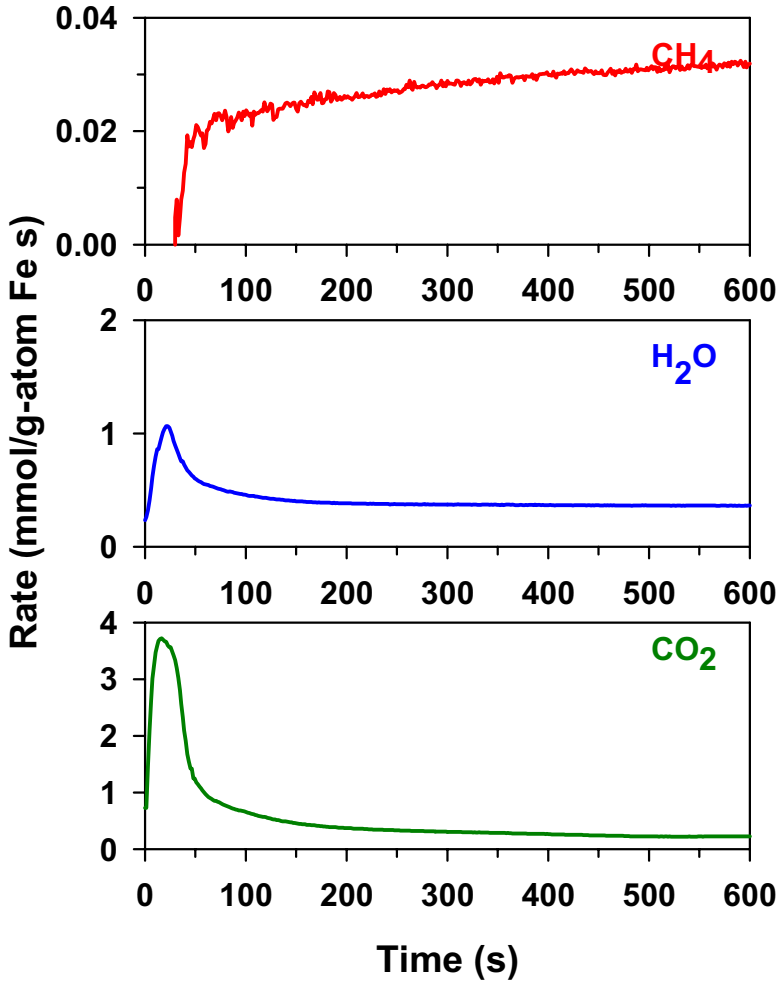

Figure 1.10 Isothermal product transients of Fe-Zn-Ru1-K2 oxide (0.2g, Zn/Fe=0.1, Ru/Fe=0.01, K/Fe=0.02) in synthesis gas (H_2/CO=2, 60 % synthesis gas in Ar, total flow rate 100 cm^3/min) at 523 K.

4. FISCHER-TROPSCH SYNTHESIS ON IRON CATALYSTS

4.1. Catalyst Loading and Activation

During this reporting period, Ru-promoted Fe-Zn catalysts were tested for the FTS reaction at a H_2/CO ratio of 2:1. The catalyst sample (80-140 mesh, 0.2 g) was diluted with quartz chips in order to avoid temperature gradients. The quartz chips were washed with diluted nitric acid and treated in air at 600 ^oC for 3 hr, before use. The total bed volume, including catalyst and quartz chips, was 8 cm^3 to give a bed height of 8 cm. Temperatures were recorded along the catalyst bed during FT synthesis. It was found that temperatures were within ±0.5 ^oC of the average axial temperature and the average axial temperature was within ±0.2 ^oC of the desired set point. For all runs, the catalyst was activated before FT synthesis reaction. Activation was carried out *in situ* by heating the catalyst in synthesis gas (62% H_2, 31% CO and 7% N_2) at 1 atm by increasing the temperature from 20 ^oC to 270 ^oC at a rate of 1 ^oC/min and holding it at 270^oC for a period of 1 hour. Following this step, the reactor temperature and pressure were set to the desired reaction conditions.

4.2. FTS Reactions over Fe-Zn-Ru

The key shortcoming of the Fe-Zn-Cu-K system that has been studied at depth previously is that it has a significant water gas-shift reaction activity. During this quarter, we have attempted to replace Cu, which is the best-available low-temperature water gas-shift catalyst, with Ru on Fe-Zn for the FTS reaction. The principal reason for exploring the Ru-promoted system was to probe the behavior of this catalyst towards the FT reaction as well as the possible minimization of the CO_2 selectivity. Ru-based catalysts have been widely studied for application in FT synthesis and also been used as promoters on Co-based catalysts [28-31]; hence Ru was an attractive option for our experiments.

The FTS reaction was carried out on a Fe-Zn-Ru catalyst (Zn/Fe=0.1, Ru/M=0.01) and its catalytic properties are compared in this section with those of a Fe-Zn-Cu catalyst (Zn/Fe=0.1, Cu/M=0.01) studied previously [19-20]. CO conversions on these two catalysts as a function of the reciprocal CO space velocity collected at 235^oC and 21.4 atm are shown in Fig. 1.11. The Ru-based catalyst has a much higher activity than the Cu-promoted catalyst. Our TPSR studies with Fe-Zn-Ru have shown that the presence of Ru promotes the reduction and carburization on the catalyst, which appears to lead to higher CO conversion and rates.

Water and CO_2 are both primary oxygenate products of the FT synthesis, but CO_2 can also form *via* subsequent secondary water-gas shift reactions. CO_2 can be formed in the primary steps *via* the removal of oxygen atoms from the catalyst surface using CO after the CO dissociation step that also forms -CH_x monomers. The CO_2 selectivities are shown as a function of the CO conversion on the two catalysts in Fig. 1.12. The CO_2 selectivity increased with CO conversion and it was higher on Fe-Zn-Ru than Fe-Zn-Cu. It is also observed that the slopes of the CO_2 selectivity curves, which are a measure of CO_2 formation *via* the secondary water gas-shift reaction, are different at low CO

conversions but identical at high CO conversions. Thus, the rate of the water-gas shift reaction appears to be slightly higher on the Ru-based catalyst at low CO conversions. At high conversions, the difference between the two systems is dictated by the primary CO_2 formation, *i.e.*, the removal of CO as CO_2. The Ru-promoted catalysts appear to be more effective than the Cu-promoted counterparts for the water gas-shift reaction.

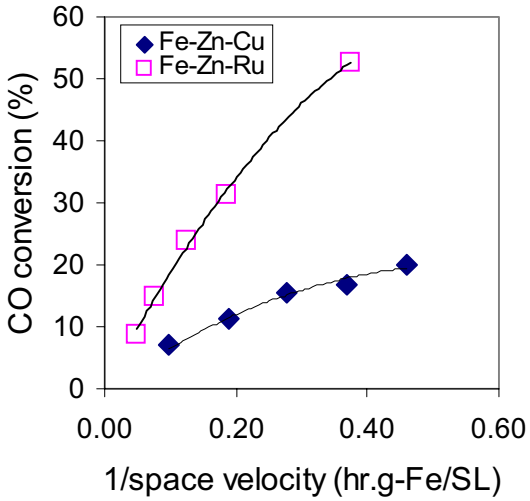

Fig. 1.11. CO conversion as a function of reciprocal space velocity for the catalysts; Fe-Zn-Ru (Zn/Fe=0.1, Ru/M=0.01) and Fe-Zn-Cu (Zn/Fe=0.1, Cu/M=0.01) at 235^{o}C and 21.4 atm, H_2/CO=2.

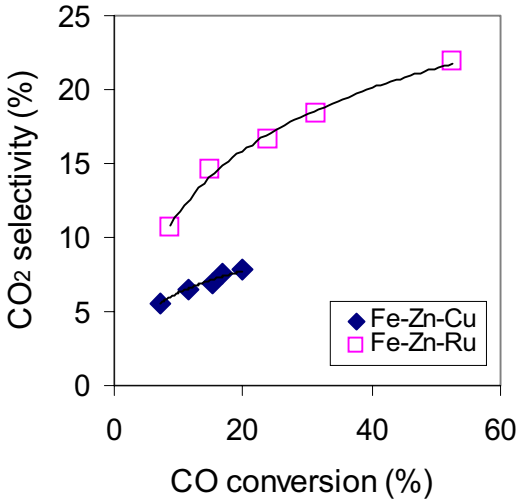

Fig. 1.12. CO_2 selectivity as a function of CO conversion for different Fe-based catalysts; Fe-Zn-Ru (Zn/Fe=0.1, Ru/M=0.01) and Fe-Zn-Cu (Zn/Fe=0.1, Cu/M=0.01) at 235^{o}C and 21.4 atm, H_2/CO=2.

A comparison of methane selectivities on the two catalysts is shown as a function of CO conversion in Fig. 1.13. The methane selectivity is lower on Fe-Zn-Ru. The C_{5+} selectivity is higher on Fe-Zn-Ru catalysts (Fig. 1.14). The presence of Ru on the Fe-Zn surface increases the concentration of the carbon species, which results in a decrease in

methane formation and enhances chain growth leading to the formation of heavier hydrocarbons.

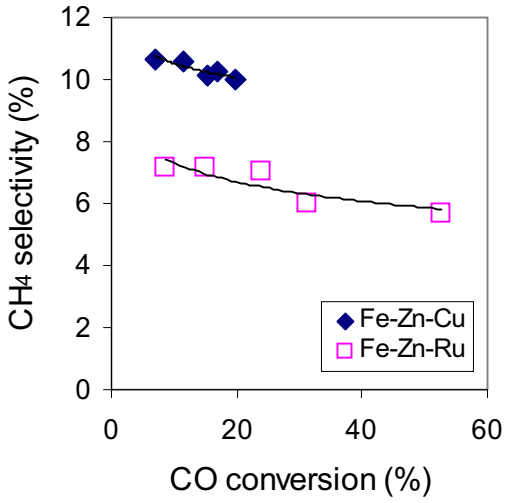

Fig. 1.13. Methane selectivity as a function of CO conversion for different Fe-based catalysts; Fe-Zn-Ru (Zn/Fe=0.1, Ru/M=0.01) and Fe-Zn-Cu (Zn/Fe=0.1, Cu/M=0.01) at 235°C and 21.4 atm, H_2/CO=2.

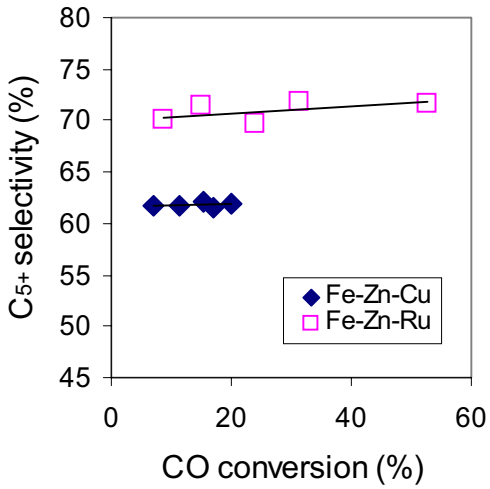

Fig. 1.14. C_{5+} selectivity as a function of CO conversion for different Fe-based catalysts; Fe-Zn-Ru (Zn/Fe=0.1, Ru/M=0.01) and Fe-Zn-Cu (Zn/Fe=0.1, Cu/M=0.01) at 235°C and 21.4 atm, H_2/CO=2.

Primary α-olefin products undergo secondary hydrogenation to form *n*-paraffins. The reactivity of α-olefin increases with increasing carbon number, while the residence time of α-olefins within the catalyst pellets also increases with increasing carbon number because of transport restrictions; hence, olefins with higher carbon number have a greater chance to hydrogenate. The α–olefin/*n*-paraffin ratio for the two catalysts is shown as a function of carbon number in Fig. 1.15. Fe-Zn-Ru products had a higher olefin content than the corresponding Fe-Zn-Cu ones. The *1*-pentene/*n*-pentane ratio for the two catalysts at 235°C and 21.4 atm are shown in Fig. 1.16 as a function of reciprocal CO space velocities. Both catalysts had a *1*-butene/*n*-butane ratio that was almost unchanged

with space time. The y-intercept of this curve is a measure of the intrinsic olefin-paraffin termination, while the slope of the curve is a measure of the secondary hydrogenation/readsorption and chain growth. The slope of the curve for Fe-Zn-Ru was almost zero indicating that the catalyst exhibited no secondary hydrogenation reaction whereas on the Cu catalyst, there was a significant olefin hydrogenation. The difference in the y-intercept values also indicated a difference in the intrinsic olefin-paraffin termination characteristics, which suggest that the Ru-containing catalyst has a lower (H*/CO*) surface ratio than the Cu-promoted catalysts. Such a proposal is also consistent woth the more prevalent removal of surface oxygen species by CO rather than hydrogen on Ru-containing catalysts as discussed earlier.

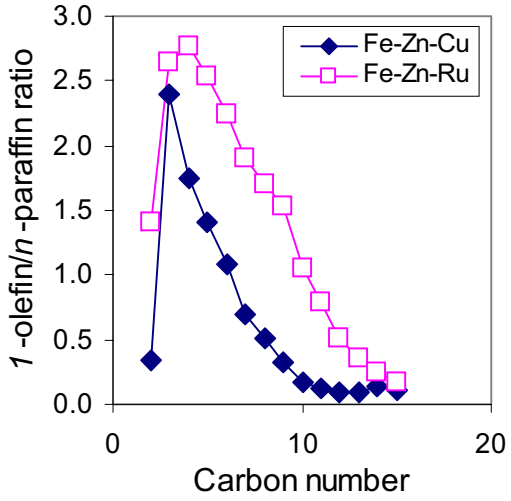

Fig. 1.15. α-olefin/*n*-paraffin ratio as a function of the carbon number for the FTS reaction for the different Fe-based catalysts at 15% CO conversion; Fe-Zn-Ru (Zn/Fe=0.1, Ru/M=0.01) and Fe-Zn-Cu (Zn/Fe=0.1, Cu/M=0.01) at 235^{o}C and 21.4 atm, H_2/CO=2.

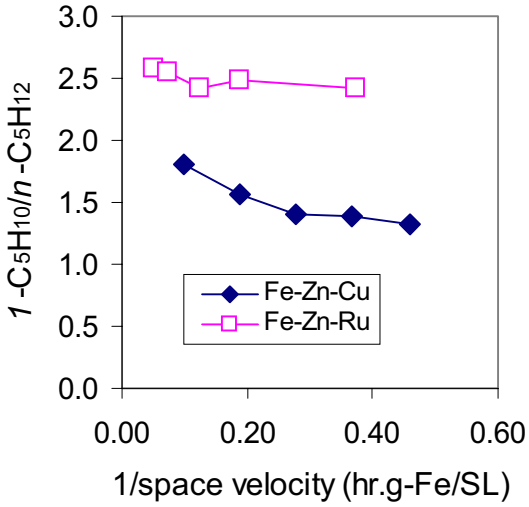

Fig. 1.16. *1*-pentene/*n*-pentane ratio as a function of reciprocal space velocity for the Fe-Zn-Ru (Zn/Fe=0.1, Ru/Fe=0.01) and Fe-Zn-Cu (Zn/Fe=0.1, Cu/M=0.01) catalysts at 235^{o}C and 21.4 atm, H_2/CO=2.

4.3. Investigation of K Effects on FTS Reaction

We have reported in the previous section that the promotion of Fe-Zn by Ru led to a significant improvement in the FTS reaction rates and led to lower CH_4 selectivities when compared with the corresponding Cu-promoted catalyst [19]. Our next step was to study the effects of K addition on the Fe-Zn-Ru system and compare it to Fe-Zn-Cu-K studied previously [20].

Previous studies on FT synthesis on Fe-based catalysts have shown that the presence of K increases the FTS and water-gas shift rates [14,17,19,24]. Potassium donates electrons to iron, thus increasing CO chemisorption energies, because CO adsorption benefits from the higher resulting electron density near from Fe atoms. In contrast, hydrogen donates electrons to iron (electron affinity decreases upon H_2 chemisorption), and the presence of the electron-donating alkali should weaken Fe-H bonds. The net result of potassium promotion is the strengthening of the Fe-C bond and the weakening of C-O and Fe-H bonds [25]. The weakening of C-O bond favors its dissociation and the removal of oxygen by hydrogen to form $-CH_x$ monomers, an essential step in the FTS catalytic sequence.

The CO conversions obtained on both the K-promoted and non-promoted Fe-Zn-Ru catalysts at 235 ^oC and 270 ^oC are shown as a function of reciprocal space velocity in Figures 1.17 and 1.18. The addition of K increased CO conversions on Fe-Zn-Ru at 235 ^oC, while at 270 ^oC, the CO conversion decreased upon K addition.

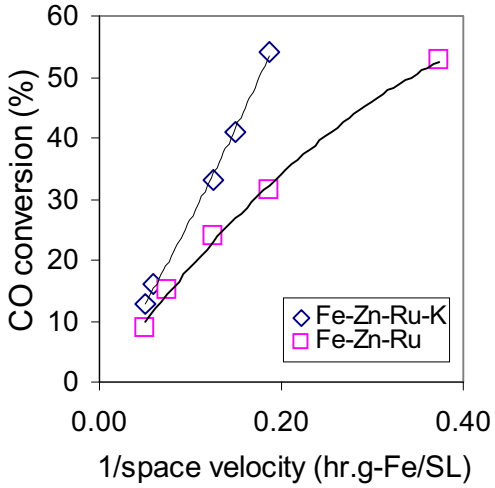

Fig. 1.17. CO conversion as a function of reciprocal space velocity for the catalysts; Fe-Zn-Ru (Zn/Fe=0.1, Ru/M=0.01) and Fe-Zn-Ru-K (Zn/Fe=0.1, Ru/M=0.01, K/M=0.02) at 235 ^oC and 21.4 atm, $H_2/CO=2$.

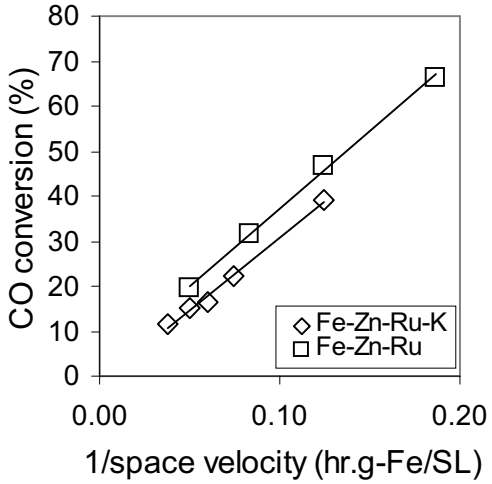

Fig. 1.18. CO conversion as a function of reciprocal space velocity for the catalysts; Fe-Zn-Ru (Zn/Fe=0.1, Ru/M=0.01) and Fe-Zn-Ru-K (Zn/Fe=0.1, Ru/M=0.01, K/M=0.02) at 270 ^oC and 5 atm, $H_2/CO=2$.

Table 1 contains a summary of the FTS reaction data for the non-promoted and K-promoted Fe-Zn-Cu and Fe-Zn-Ru catalysts. At the same CO space velocity, CO conversion rates are higher on the K-promoted catalysts than on the non-promoted catalysts at the low temperature. At 270 ^{o}C, the CO conversions and rates were almost unchanged upon K-addition for the Fe-Zn-Cu, while they decreased in the case of Fe-Zn-Ru.

The FTS reaction rate is determined by the effective surface concentration of hydrogen and carbon species on the catalyst surface. K promotes the dissociation of CO and prevents the chemisorption of hydrogen, while Ru promotes the dissociation of hydrogen on the catalyst. It is possible that a favorable hydrogen/carbon surface concentration exists at low temperatures in the presence of both Ru and K at the lower temperature, which could explain the higher CO conversion on the K-promoted catalyst. On the other hand at the higher temperature, the behavior of the catalyst mirrors that of the Fe-Si system, which showed a decrease in the conversion upon K addition [16,19,26]. K facilitates carbon deposition on the catalyst surface and this process is enhanced at the high temperature. Thus it is possible that some of the active sites may be covered leading to a lower CO rate at 270 ^{o}C on the K-promoted catalysts. This effect appears to be stronger on Fe-Zn-Ru than Fe-Zn-Cu.

Table 1: Effects of K promotion on Fe-Zn-Ru and Fe-Zn-Cu for the FTS reaction at different conditions

	235^{o}C, 21.4 atm				**270^{o}C, 21.4 atm**			
	Fe-Zn-Ru	Fe-Zn-Ru-K	Fe-Zn-Cu	Fe-Zn-Cu-K	Fe-Zn-Ru	Fe-Zn-Ru-K	Fe-Zn-Cu	Fe-Zn-Cu-K
Space velocity (Nl/hr.g-Fe)	13.4	16.7	2.2	5.3	20.1	13.4	5.4	5.3
CO conversion (%)	14.9	15.9	19.9	21.8	19.5	22.3	20.5	21.8
CO rate (mol/hr.mol-Fe)	4.7	6.3	1.1	2.7	9.2	7.0	2.8	2.7
CO rate to CO_2 (mol/hr.mol Fe)	0.7	1.5	0.1	0.7	2.7	3.2	0.7	1.1
CO rate to HC (mol/hr.mol Fe)	4.0	4.8	1.0	2.0	6.5	3.8	2.1	1.6
HC productivity (g/hr.kg-Fe)	1007	1191	256	509	1642	958	518	398
HC selectivity - CO_2 free								
CO_2 selectivity (%)	14.6	24.3	7.8	24.2	29.1	45.8	25.3	40.7
CH_4 selectivity (%)	7.1	3.1	10	2.2	11.0	5.3	15.1	10.4
C_{5+} selectivity (%)	71.4	86.8	62	86.2	63.0	77.2	50.4	63.5
1-C_7H_{14}/*n*-C_7H_{16} ratio	1.9	2.1	0.6	2.3	2.1	4.1	0.5	3.3

The CO_2 selectivity also is higher on the K-promoted catalysts and it increased with increasing temperature. As observed before in the case of Fe-Si, the effect of K appears to be to increase the primary rate of CO_2 formation, *i.e.*, from CO. Methane selectivities are lower on the K-promoted catalyst, while the C_{5+} selectivities were higher at both 235 ^{o}C and 270 ^{o}C. The lower CH_4 and higher C_{5+} selectivity numbers appear to reflect the higher CO and lower hydrogen surface coverages in the presence of potassium, which favor chain growth. K promotes CO chemisorption and inhibits H_2 chemisorption on the catalyst surface.

K influences the α-olefin/*n*-paraffin ratios by decreasing the surface hydrogen coverage and inhibits secondary hydrogenation reactions. K also helps to titrate acid sites on the catalyst thus minimizing secondary isomerization reactions. *1*-heptene/*n*-heptane ratios increased upon K addition on all the catalysts. At 235 ^{o}C, this change was much smaller than at 270 ^{o}C on Fe-Zn-Ru. K facilitates carbon deposition at the higher temperature, which could possibly cover some of the Ru, thus leading to a decrease in the net hydrogen available on the catalyst. It is also possible that the catalyst may undergo sintering and the Ru-component may be oxidized at the higher temperature, which could explain the differences.

4.4. Comparison of the different Fe Catalysts for the FTS Reaction

In this section, a comparison of the performance of the best three Fe catalysts studied thus far, Fe-Zn-Ru-K, Fe-Zn-Cu-K and Fe-Si-K are presented [19,23]. The CO conversions on all the Fe-based catalysts as a function of the reciprocal CO space velocity collected at 235^{o}C and 21.4 atm are shown in Fig. 1.19. The Ru-promoted catalyst appears to have the highest CO conversion rates among all the catalysts studied. The CO_2 selectivities are shown as a function of the CO conversion on the two catalysts in Fig. 1.20. The CO_2 selectivity increased almost linearly with CO conversion values and is similar for both Fe-Zn-Cu-K and Fe-Zn-Ru-K and significantly higher than on Fe-Si-K. The slopes of the CO_2 selectivity curves are almost identical for all the catalysts and the only difference is in the y-intercepts. This shows that both the Cu and Ru-promoted systems have a higher rate of removal of CO_2 directly from CO. This difference appears to be due to a lower effective K concentration on the Fe-Si-K (K/M=1.44) compared to the other systems (K/M=0.02).

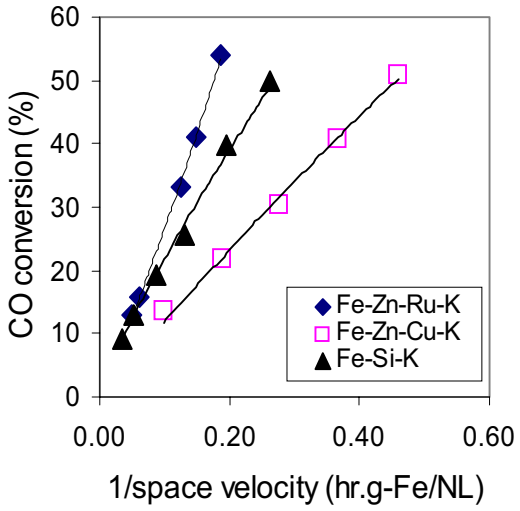

Fig. 1.19. CO conversion as a function of reciprocal space velocity for different Fe-based catalysts; Fe-Si-K (Si/Fe=0.046, K/Fe=0.014), Fe-Zn-Ru-K (Zn/Fe=0.1, Ru/M=0.01, K/M=0.02) and Fe-Zn-Cu-K (Zn/Fe=0.1, Cu/M=0.01, K/M=0.02) at 235^{o}C and 21.4 atm, H_2/CO=2.

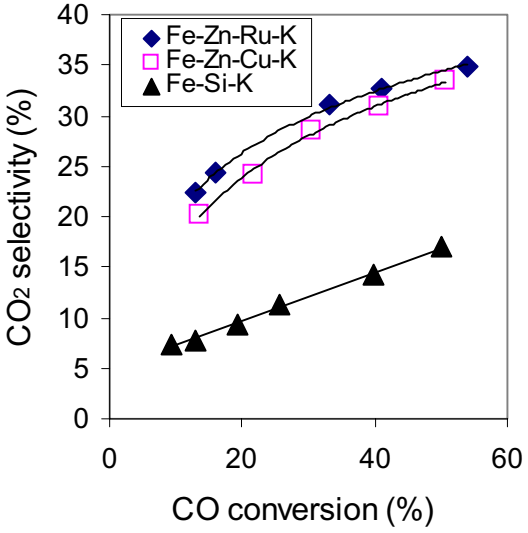

Fig. 1.20. CO_2 selectivity as a function of CO conversion for different Fe-based catalysts; Fe-Si-K (Si/Fe=0.046, K/Fe=0.014), Fe-Zn-Ru-K (Zn/Fe=0.1, Ru/M=0.01, K/M=0.02) and Fe-Zn-Cu-K (Zn/Fe=0.1, Cu/M=0.01, K/M=0.02) at 235^{o}C and 21.4 atm, H_2/CO=2.

A comparison of methane selectivities on the two catalysts is shown as a function of CO conversion in Fig. 1.21. The methane selectivity is similar on the Cu and Ru-systems and much lower than Fe-Si-K. The difference is due to the stronger effect of K in reducing H_2 chemisorption on the catalyst in the case of Fe-Zn-Cu and Fe-Zn-Ru.

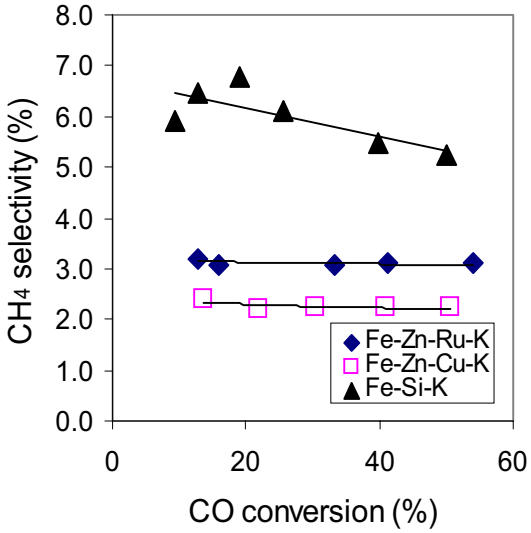

Fig. 1.21. Methane selectivity as a function of CO conversion for different Fe-based catalysts; Fe-Si-K (Si/Fe=0.046, K/Fe=0.014), Fe-Zn-Ru-K (Zn/Fe=0.1, Ru/M=0.01, K/M=0.02) and Fe-Zn-Cu-K (Zn/Fe=0.1, Cu/M=0.01, K/M=0.02) at 235 ^{o}C and 21.4 atm, H_2/CO=2.

The results for all these catalysts at all the reaction conditions are summarized in Tables 2 and 3. The Fe-Zn-Ru-K and Fe-Si-K catalysts exhibit higher reaction rates and HC productivities than the Cu-promoted system at both the reaction conditions. Although the

CO rates are higher on the Ru-based catalyst than Fe-Si-K, they both exhibit similar HC productivities because of the lower CO_2 selectivities on Fe-Si-K. Both Fe-Zn-Ru and Fe-Zn-Cu show high CO_2 selectivities than Fe-Si-K due to higher primary CO_2 formation rates. The performance of the Fe-Si-K is limited by its lower selectivity to C_{5+} hydrocarbons especially at the low temperature. It is however interesting to note that the Ru system retains its high C_{5+} selectivity even at 270 ^oC, in contrast to the Cu-based catalyst. The *1*-pentene/*n*-pentane ratio is very similar for all the catalysts at a given CO conversion.

Table 2. A comparison of the FTS reaction parameters at 235 ^oC, 21.4 atm and 270 ^oC, 5 atm for all the Fe-based catalysts tested

	235^{o}C, 21.4 atm			**270^{o}C, 21.4 atm**		
	Fe-Zn-Ru-K	Fe-Zn-Cu-K	Fe-Si-K	Fe-Zn-Ru-K	Fe-Zn-Cu-K	Fe-Si-K
Space velocity (Nl/hr.g-Fe)	16.7	5.3	11.5	13.4	5.3	19.1
CO conversion (%)	15.9	21.8	19.2	22.3	21.8	19.9
CO rate (mol/hr.mol-Fe)	6.3	2.7	5.5	7.0	2.7	9.5
CO rate to CO_2 (mol/hr.mol Fe)	1.5	0.7	0.5	3.2	1.1	2.9
CO rate to HC (mol/hr.mol Fe)	4.8	2.0	5.0	3.8	1.6	6.6
HC productivity (g/hr.kg-Fe)	1191	509	1246	958	398	1652
HC selectivity - CO_2 free						
CO_2 selectivity (%)	24.3	24.2	9.4	45.8	40.7	30.6
CH_4 selectivity (%)	3.1	2.2	6.8	5.3	10.4	8.2
C_{5+} selectivity (%)	86.8	86.2	72.9	77.2	63.5	67.5
1-C_7H_{14}/*n*-C_7H_{16} ratio	2.1	2.3	2.4	4.1	3.3	3.9

Table 3. A comparison of the FTS reaction parameters at 220 ^oC, 31.6 atm for all the Fe-based catalysts tested

	220^{o}C, 31.6 atm		
	Fe-Zn-Ru-K	Fe-Zn-Cu-K	Fe-Si-K
Space velocity (Nl/hr.g-Fe)	10.0	5.3	7.6
CO conversion (%)	17.8	16.2	21.0
CO rate (mol/hr.mol-Fe)	4.2	2.0	4.0
CO rate to CO_2 (mol/hr.mol Fe)	0.8	0.3	0.3
CO rate to HC (mol/hr.mol Fe)	3.4	1.7	3.7
HC productivity (g/hr.kg-Fe)	861	438	928
HC selectivity - CO_2 free			
CO_2 selectivity (%)	18.6	12.3	7.5
CH_4 selectivity (%)	2.6	1.8	4.6
C_{5+} selectivity (%)	85.5	87.6	77.0
1-C_7H_{14}/*n*-C_7H_{16} ratio	1.6	1.7	1.9

Based on the results shown in Table 2, Fe-Zn-Ru-K appears to be the best catalyst for the FTS reaction among all the catalysts studied. Inspite of having a high selectivity to CO_2, this catalyst has a high hydrocarbon productivity. Our next step is study further the optimum Ru loading required for good performance from an economic standpoint and the effects of thermal pretreatment on the dispersion and effectiveness of the Ru component. Furthermore, this catalyst is attractive from the point of being used as a low temperature FTS catalyst and studies are underway to study this effect.

II. FISCHER-TROPSCH SYNTHESIS ON COBALT CATALYSTS

1. Analysis of Kinetic Data

We had been working on a multivariable non-linear regression program based on the least squares approach designed for the elucidation of Fischer-Tropsch reaction kinetics. This program has been completed using Matlab and it was used to test the different kinetic rate expressions developed for several possible sequences of elementary steps for the Co/SiO_2 system using the kinetic data previously reported [20-21].

We had proposed a rate mechanism that would explain the enhancement of synthesis rate by water observed on cobalt catalysts [21]. This mechanism took into account the fact that the surface of Co is almost entirely covered by non-dissociated CO [32-33]. Hence the dissociation of CO by adsorbed hydrogen and water to form C*, which could control the overall CO consumption rate, were taken as elementary steps in the mechanism.

Mechanism 1:

1. $H_2 + 2* \Leftrightarrow 2H*$
2. $CO + * \Leftrightarrow CO*$
3. $CO* + H* \Rightarrow C* + OH*$
4. $CO* + OH_2* \Rightarrow C* + 2OH*$
5. $O* + H* \Rightarrow OH* + *$
6. $OH* + H* \Rightarrow OH_2* + *$
7. $OH_2* \Leftrightarrow H_2O + *$

The above mechanism led to the following rate expression,

$$r_{CO} = \frac{\left(aP_{CO}P_{H_2}{}^{1/2} + bP_{CO}P_{H_2O}\right)}{\left(1 + cP_{H_2}{}^{1/2} + dP_{H_2O} + eP_{CO}\right)^2}$$

This rate expression has a positive order dependence on water and has a negative CO order at high CO coverage. The kinetic data obtained on the 21.9% Co/SiO_2 during the previous quarters was used in the regression program [20-21]. The data appears to be consistent with the above rate expression and the values of the parameters a-e were as follows.

a = 59.8 $atm^{-3/2}$ hr^{-1}
b = 527.1 atm^{-2} hr^{-1}
c = $2.3*10^{-14}$ $atm^{-1/2}$
d = 1.8 atm^{-1}
and e = 1.0 atm^{-1}

Another mechanism had also been considered by including an additional step that would account for the possibility of formation of CH* directly during hydrogen-assisted CO dissociation [22].

Mechanism 2:

1. $H_2 + 2* \Leftrightarrow 2H*$
2. $CO + * \Leftrightarrow CO*$
3. $CO* + H* \Rightarrow C* + OH*$
4. $CO* + H* \Rightarrow CH* + O*$
5. $CO* + OH_2* \Rightarrow COH* + 2OH*$
6. $COH* + * \Rightarrow C* + OH*$
7. $O* + H* \Rightarrow OH* + *$
8. $OH* + H* \Rightarrow OH_2* + *$
9. $OH_2* \Leftrightarrow H_2O + *$

The parallel pathways for CO dissociation are described by the steps 3, 4 and 5. This mechanism led to the following rate expression.

$$r_{CO} = \frac{\left(aP_{CO}P_{H_2}^{1/2} + bP_{CO}P_{H_2O}\right)}{\left(1 + cP_{H_2}^{1/2} + dP_{H_2O} + eP_{CO} + \frac{fP_{CO}P_{H_2O}}{P_{H_2}^{1/2}}\right)^2}$$

where the rate is given in hr^{-1} and the individual pressures in atm. The experimental data was also used to test the above expression in the regression program and determine the various constants. The values of the different parameters obtained were as follows:

$a = 45.3\ atm^{-3/2}\ hr^{-1}$
$b = 443.4\ atm^{-2}\ hr^{-1}$
$c = 8.8*10^{-8}\ atm^{-1/2}$
$d = 1.5*10^{-8}\ atm^{-1}$
$e = 0.9\ atm^{-1}$
and $f = 1.0\ atm^{-3/2}$

A comparison between the measured rates and predicted rates is plotted for both the above-mentioned mechanisms is shown in Figures 1.22 and 1.23. In both cases, the predicted rates are within 95% of the measured rates and hence both the mechanisms are consistent with the FTS reaction kinetics on Co/SiO_2 and can explain the positive water effect on these catalysts.

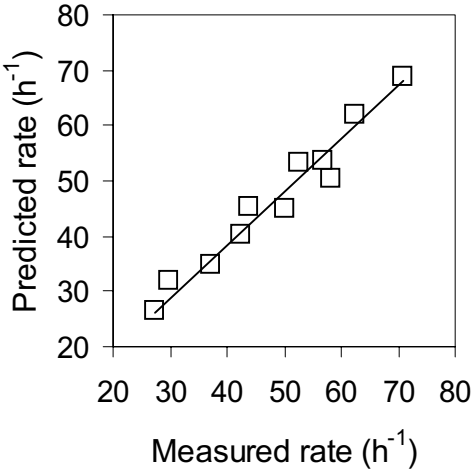

Fig. 1.22. A comparison of predicted rates from Mechanism 1 with the measured rates for a 21.9% Co/SiO_2 catalyst at 200°C and 20 atm, $H_2/CO=2$.

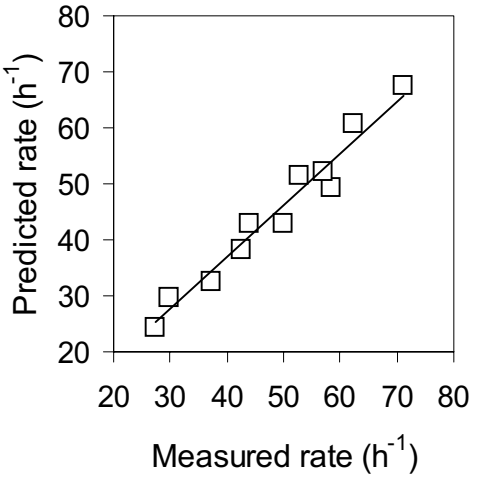

Fig. 1.23. A comparison of predicted rates from Mechanism 2 with the measured rates for a 21.9% Co/SiO_2 catalyst at 200°C and 20 atm, $H_2/CO=2$.

2. Runs with a 21.9% Co/SiO_2 Catalyst

We had previously reported discrepancies in hydrocarbon selectivities with the 21.9% Co/SiO_2 catalyst for the FT reaction, during our attempts to certify the reactor for normal operation. During this reporting period, the gas chromatograph was recalibrated with a certified gas mixture containing C_1-C_4 hydrocarbons, CO, CO_2 and N_2, and the TCD response factors were recalculated. The TCD response factors for CH4 and CO were found to be significantly different from the old values upon recalibration with the certified standard.

The experiments were repeated with the 21.9% Co/SiO_2 catalyst at 200°C and 20 atm. The site-time yields obtained during these experiments are compared in Figure 1.24 with the earlier data [19]. The rates are almost identical in both cases. Figure 1.25 and 1.26 show the CH_4 and C_{5+} selectivities in both cases. It appears that there are still some small differences in the data but the new data appears to mirror selectivity numbers obtained before on similar catalysts [34].

The α-olefin/*n*-paraffin ratios for different space velocities are shown as a function of carbon number in both cases in Figures 1.27 and 1.28. The comparison shows that the catalyst appears to slightly more hydrogenating in the case of the new data. These numbers again are similar to those reported earlier in the literature on Co catalysts [34]. The remaining differences in the CH_4 selectivity and α-olefin/*n*-paraffin ratios are possibly due to hydrogenation reactions on the wall of the reactor. Tests with an empty

reactor revealed the formation of a small amount of methane. It is possible that the olefins are hydrogenated on the walls of the reactor leading to a lower α-olefin/*n*-paraffin ratio. Further tests will be conducted with a different reactor to test the hydrogenation effect.

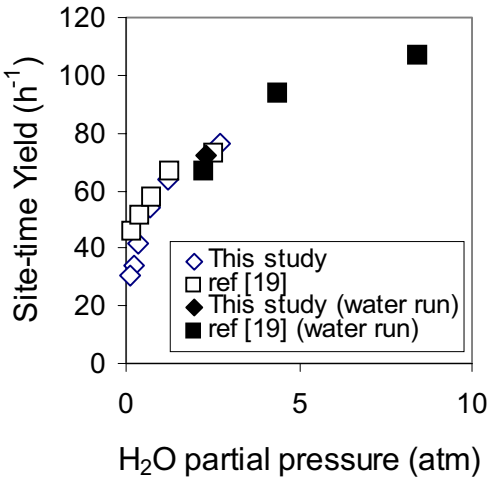

Fig. 1.24. A comparison of the Co site-time yields on the 21.9% Co/SiO_2 catalyst at 200°C and 20 atm, $H_2/CO=2$.

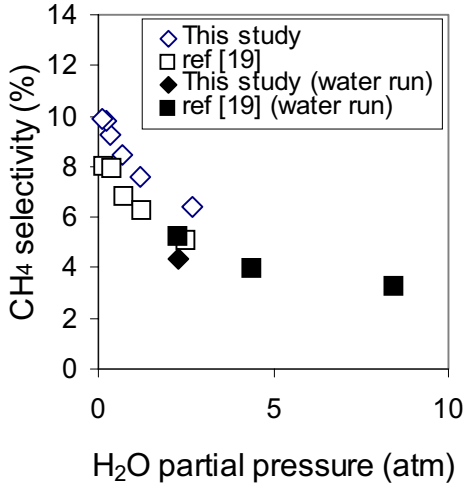

Fig. 1.25. A comparison of the CH_4 selectivities as a function of H_2O partial pressure on the 21.9% Co/SiO_2 catalyst at 200°C and 20 atm, $H_2/CO=2$.

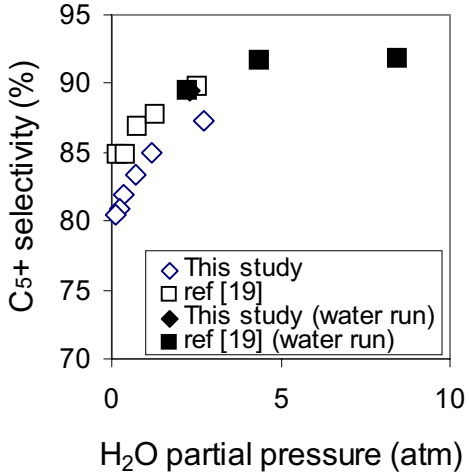

Fig. 1.26. A comparison of the C_{5+} selectivities as a function of H_2O partial pressure on the 21.9% Co/SiO_2 catalyst at 200°C and 20 atm, $H_2/CO=2$.

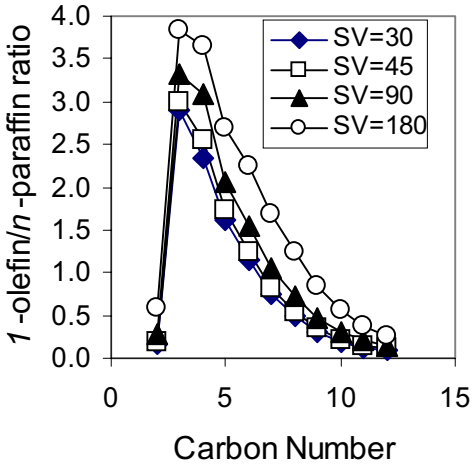

Fig. 1.27. α-olefin/*n*-paraffin ratios as a function of carbon number at different space velocities on the 21.9% Co/SiO_2 catalyst at 200°C and 20 atm, $H_2/CO=2$. This study.

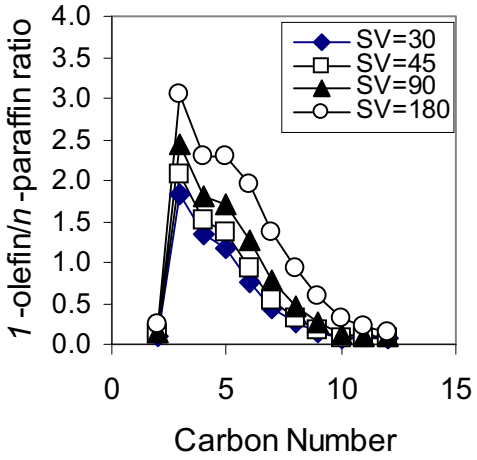

Fig. 1.28. α-olefin/*n*-paraffin ratios as a function of carbon number at different space velocities on the 21.9% Co/SiO_2 catalyst at 200°C and 20 atm, $H_2/CO=2$. Ref [19].

II. APPENDIX

1. References

1. M. E. Dry, The Fisher-Tropsch Synthesis, in *Catalysis-Science and Technology*, Vol. 1, p. 160, J. R. Anderson and M. Boudart eds., Springer Verlag, New York, 1981.
2. F. Fischer and H. Tropsch, *Brennstoff-Chem.* 7 (1926) 97.
3. R. B. Anderson, in *Catalysis* Vol. 4, p. 29, P. H. Emmett eds., Van Nostrand-Reinhold, New York, 1956.
4. H. H. Storch, N. Golumbic and R. B. Anderson, *The Fischer-Tropsch and Related Syntheses*, Wiley, New York, 1951; R. B. Anderson, *The Fischer-Tropsch Synthesis*, Wiley, New York, 1984.
5. H. Kolbel and M. Ralek, *Catal. Rev.-Sci. Eng.* 21 (1980) 225.
6. J. W. Niemantsverdriet and A. M. van der Kraan, *J. Catal.* 72 (1981) 385.
7. J. A. Amelse, J. B. Butt and L. J. Schwartz, *J. Phys. Chem.* 82 (1978) 558.
8. G. B. Raupp and W. N. Delgass, *J. Catal.* 58 (1979) 348.
9. R. Dictor and A. T. Bell, *J. Catal.* 97 (1986) 121.
10. J. P. Reymond, P. Meriaudeau and S. J. Teichner, *J. Catal.* 75 (1982) 39.
11. C. S. Kuivila, P. C. Stair and J. B. Butt, *J. Catal.* 118 (1989) 299.
12. C. S. Huang, L. Xu and B. H. Davis, *Fuel Sci. Tech. Int.* 11 (1993) 639.
13. S. Soled, E. Iglesia and R. A. Fiato, *Catal. Lett.* 7 (1990) 271.
14. S. Soled, E. Iglesia, S. Miseo, B. A. DeRites and R. A. Fiato, *Topics in Catal.* 2 (1995) 193.
15. E. Iglesia, A research proposal submitted to the Division of Fossil Energy.
16. R. J. O'Brien, L. Xu. R. L. Spicer and B. H. Davis, *Energy and Fuels*, 10 (1996) 921.
17. D. B. Bukur, D. Mukesh, and S. A. Patel, *Ind. Eng. Chem. Res*., 29, 194 (1990).
18. 1st Quarterly report, 1999. U.S. Department of Energy under contract # DE-FC26-98FT40308.
19. 2nd Quarterly report, 1999. U.S. Department of Energy under contract # DE-FC26-98FT40308.
20. 3rd Quarterly report, 1999. U.S. Department of Energy under contract # DE-FC26-98FT40308.
21. 4th Quarterly report, 1999. U.S. Department of Energy under contract # DE-FC26-98FT40308.
22. 1st Quarterly report, 2000. U.S. Department of Energy under contract # DE-FC26-98FT40308.
23. 2nd Quarterly report, 2000. U.S. Department of Energy under contract # DE-FC26-98FT40308.
24. H. Kolbel, in Actes du Deuxieme Congres Internationale de Catalyse, Tchinp, Paris, 1960; Vol. II, 2075-2099.
25. J. Benziger, and R. Madix, *Surf. Sci. Catal*., 109 (1981) L527.
26. A. P. Raje, R. J. O'Brien, and B. H. Davis, *J. Catal*., 180 (1) (1998) 36.
27. R. C. Brady, and R. Pettit*, J. Am. Chem. Soc.*, 103 (1981) 1287.
28. D.O. Uner,, M. Pruski, and T.S. King, *Topics in Catalysis*, 2 (1995) 59.
29. R.A. Dalla Betta, and M. Shelef, *J. Catal*., 48 (1977) 111.
30. C.S. Kellner, and A.T. Bell, *J.Catal*., 70 (1981) 418.

31. E. Iglesia, S.L. Soled, R.A. Fiato, and G.H. Via, *J. Catal.*, 143 (1993) 345.
32. H.H. Storch, N. Golumbic, and R.B. Anderson, *The Fischer-Tropsch and related syntheses*, Wiley, New York, 1951; R.B. Anderson, *The Fischer-Tropsch Synthesis*, Wiley, New York, 1984.
33. A.T. Bell, *Catal. Rev. Sci. Eng.*, 23 (1-2) (1981) 203.
34. E. Iglesia, *Appl. Catal. A*, 161 (1997) 59.

Task 12. Reporting/Project Management

Three monthly and one quarterly reports have been completed.